Author response to Marijn Floris van Dooren

The authors response is shown in red.
Changes implemented in the new version of the manuscript are in blue.

This paper presents an interesting study on the characterisation and validation of analytical yawed wake models. The writing is of high quality, the figures are nice and in general the paper is very informative. However, in some aspects the paper could be a bit more 'to the point'. I will illustrate that with further comments. I suggest a minor revision.

We thank Dr. van Dooren for his comments, which helped to improve the manuscript. Based on the comments from him and Prof. Barthelmie we implemented the following notable changes to the manuscript:

- The abstract and conclusion were modified to provide more room for the evaluation of the wake-steering setup.
- The validation of the inflow measurements uses the wake-steering cases and the control cases to make the usage of measurement data uniform throughout the results (Sect. 3.1).
- The validation of the analytical model distinguishes various error sources (Sect. 3.3.2)
- The effect of the wake steering on the power is estimated based on the wake-scanning lidar in addition to the analytical model (Sect. 3.4.2).
- Numerous minor changes (additions and clarification within the methods section, spelling and phrasing throughout the manuscript).

The line numbers in our replies refer to the revised manuscript. In addition to the revised manuscript, we also provide a tracked-changes manuscript that visually highlights the changes made.

General comments:

- The conclusions mainly address the errors in the power prediction for different experimental and analytical methods/models. Even the lowest value of 12% is higher than the expected power improvements reached by wake steering (Sect.3.3.3). Maybe this could be elaborated a bit more in a broader scope, addressing how these findings contribute to the research field that attempts to increase power production of turbines in an array or wind farm and what are your recommendations on how and with which methods to proceed.

  We have two points concerning the issue of the large model errors in comparison to the power increase due to wake steering:

  1. The effect of wake steering on the power is now also estimated from the wake-scanning Doppler lidar independent from the analytical model (new Fig. 14 and Table 3). These results show the same behavior as the model. Especially, a reduced wake steering success for wind directions outside a narrow sector between 325° and 335° is consistent with results of the analytical model.
  2. The increase in power due to wake steering results from the wake deflection, which the model reproduces fairly well. On the other hand, the errors of the analytical model includes the shortcomings of the power curve (one third of the error) and missing atmospheric effects (nonstationary conditions, wind veer etc.), which do not affect the findings for the increase in power directly, because it is gained from a comparison of model vs. model.

We believe the manuscript provides a meaning full contribution to the research field by demonstrating that the implemented wake steering was suboptimal and pointing out the causes. Concerning the latter, the found wind direction bias when the wind turbine is yawed is especially important, because it points to the general problem that the standard instrumentation of a wind turbine seems not sufficient to provide the required input for the wake-steering controller with the needed quality. We assume that the bias of the wind vane comes from the flow in close proximity of the nacelle while it is yawed (i.e. it is not an instrument fault, but the flow at instrument location is systematically not aligned with the wind direction of the free stream during yawed operation). We avoided drawing general conclusions about the success of wake steering, because the wake steering setup was not working as intended as mentioned above. Nevertheless, the wake steering increased the power output in some cases, but probably not as much as possible.

Using a narrower wind direction sector, to which a yaw angle offset is applied, only reduced the impact of the suboptimal wake steering, but is not an optimal solution. A correction of the bias might be possible if it only depends on the yaw angle and the wind speed. A proven solution would be a forward facing Doppler lidar to provide the input measurements (that adds other benefits, too).

The effect of wake steering on the power is computed from the wake-scanning lidar (methods on P9, L185-188; results shown in Fig. 14, Table 3, and P21, L354-359). We made changes to the abstract and conclusions to give more room for the wake steering (P24, L376-387).

- On the other hand the length of the paper could be reduced a little. I like the fact that the paper is very informative, but sometimes it provides information not directly necessary for the take-away message. One example is Sect. 3.4 on the shape of the wake. Please consider whether it is a vital concern or whether it could be omitted.

The section was included for two reasons: (i) after looking at position and depth of the wake, its shape would be the next logical property to investigate, and (ii) it provides insights on the dominant effects that are important to be considered in modeling. However, we are aware that the section is only a side note to the findings, and we decided to move the section into an appendix and reference it in the conclusions.

We moved Sect. 3.4 from the main body of the manuscript into Appendix B and referenced in the conclusions (P24, L390-391). The former Sect. 3.3 is now subdivided into a new Sect. 3.3 that only contains the model validation and a new Sect. 3.4 that contains the effect of wake steering on the power.

- You state that 'studies of yawed wind turbines using field data are rare'. Although this may be true, I recommend you to look into and perhaps cite the work of Bromm (2018), DOI: 10.1002/we.2210 in addition to the other references.

Thank you for pointing out this paper. It was extremely relevant in the context of this paper and was an interesting read.

We added Bromm et al. (2018) into the literature review of the introduction (P3, L41-42).

Specific comments:

- P2, L50: What kind of WindCube was used? There are various short-range and long-range WindCube models.

It was a WindCube-V2 profiling lidar (details have been added in Sect. 2.2.1).

Additional information on the Wind Cube added on P4, L76, and L81-82.

- P11, Fig. 5 and Fig. 6: It would be very good for the overview to see the goodness of fit (correlation) coefficient displayed within the correlations plots.

  We added quantitative information on errors and goodness of fits to all figures. Further, in response to comments of Reviewer #2, section 3.1 was modified extensively to make the usage of measurement data uniform throughout the paper.

  We included the correlation coefficient in the legends of Fig. 5. The new Fig. 6 includes the RMSE and parameters of a fitted Gaussian.

- P14, Fig. 8: Does the wake center detection function as it should? It seems to jump between the wakes of T2, T3 and T4. Wouldn't it make more sense to try to follow the far wake of T2 instead? Maybe this could be adjusted.

  Only the solid part of the white line was the successfully detected wake center. Instances where the wake center detection jumps between the wakes were detected and rejected based on the correlation threshold (the rejected parts were shown as the dashed part of the white line in the original figure).

  We removed the dashed part of the white line and show only the solid part to avoid confusion (new Fig. 9a).

- P17, Fig. 10 and Fig. 11: Again it would be nice to see the correlation coefficient displayed within the figures.

  We included the correlation coefficient and RMSE in the legends of Fig. 10 and Fig. 11.

Technical corrections:

- P2, L52: Replace 'thrid' by 'third'.

  The sentence about the third wake-scanning lidar was removed.

- P3, L59: Replace 'nacelle' by 'the nacelle'.

  Inserted "the" (P3, L64).

- P5, L82: Add 'direction' at the end of the sentence.

  Inserted "direction" (P4, L88).

- P6, L106: Replace 'StreamLine' with 'Stream Line'.

  Inserted a space (P6, L112).

- P9, L191: Rewrite 'data of either the WindIris or the WindCube was missing'.

  Corrected (P10, L208-209).

- P9, L204: Remove 'the' in front of '07 February 2019'.

  This sentence became obsolete after reworking section 3.1 to use only the wake-steering cases and control cases.

- P10, L212: Remove ’the’ in front of ’11 February 2019’.

  Removed "the" (P11, L228).

- P12, L235: Add ’a’ in front of ’mean value’.

  Inserted "a" (P13, L246).

- P14, L264: Add ’a’ in front of ’correlation coefficient’.

  After adding the correlation coefficient and RMSE to the Fig. 10, we removed this sentence.

- P16, L268: Replace ’reasons’ with ’reason’

  Removed the "s" (P15, L283).

Author response to Rebecca Barthelmie

The authors response is shown in red.
Changes implemented in the new version of the manuscript are in blue.

This paper describes a useful set of measurements used to examine wake deflection. Overall it is interesting and has a good message. It could be improved to make it substantially easier to follow and compare the different cases and data sets and models. A data access statement is required by journal policy.

We thank Prof. Barthelmie for her comments, which helped to improve the manuscript. Based on the comments from her and Dr. van Dooren we implemented the following changes to the manuscript:

- An overview of the wake-steering cases and the control cases was added the beginning of Sect. 3 (Table1).
- The validation of the inflow measurements uses the wake-steering cases and the control cases to make the usage of measurement data uniform throughout the results (Sect. 3.1).
- The validation of the analytical model distinguishes various error sources (Sect. 3.3.2)
- The effect of the wake steering on the power is estimated based on the wake-scanning lidar in addition to the analytical model (Sect. 3.4.2).
- The abstract and conclusion were modified to provide more room for the evaluation of the wake-steering setup.
- Numerous minor changes (additions and clarification within the methods section, spelling and phrasing throughout the manuscript).

The line numbers in our replies refer to the revised manuscript. In addition to the revised manuscript, we also provide a tracked-changes manuscript that visually highlights the changes made.

Please see comments below.

- Introduction: Could this be quantitative? Rather than listing the papers, wouldn't it be helpful if the introduction gave a background in terms of answering: How big are power losses due to wakes? What could be expected in terms of the gains from wake steering? What have other modeling studies and the few available field studies indicated are those magnitudes? You could then follow up in the conclusions to evaluate whether a consensus is being reached on the viability of wake steering for power gain for example.

  The power losses from wake effects depend on turbine spacing, wind direction, atmospheric stability and turbulence levels. A single fully waked wind turbine can produce 40% less power than a wind turbine in the free stream (Simley et al., 2020; Barthelmie et al. 2010). On a wind farm scale, the power losses also depend on the above mentioned variables, but additionally on how deep a wind turbine is behind the leading row of wind turbines (Barthelmie et al, 2010, Porté-Agel et al. 2013).
  For a pair of upstream-downstream turbines, the possible power improvement with wake steering given in literature ranges from 3.5% to 11% (Bartl et al. 2016) depending on turbulence levels and turbine distances. Field experiments showed values improvements of 3.5% (Simley et al. 2020) and 4% (Fleming et al. 2019).

We included quantitative information on the wake losses and the power gains with wake steering to the introduction (P1, L17-19 and P2, L29-33).

- Figure 1. The google map figure needs a scale.

  A scale was added to the overview map (P3, Fig. 1).

- Figure 2 needs an idea at least of how LONG a measurement period this represents. Is it the whole data period i.e. six months of data, from every direction?, every wind speed and turbulence condition? is it a case study?

  Figure 2 uses all available data from 6 January until 9 April 2019, which is consistent with the period used in the results. All wind speeds and turbulence levels are included as long as the wind turbine and the WindCube were operational.

  This information was added to the caption of Figure 2 (P5, Fig. 2).

- Section 2: How was the target yaw offset determined? How were the wind directions determined from the lidar data? What is the purpose of the analytical models? (beyond 'comparison with data'? what is the objective?) Please elaborate why and how you used the models. What are the errors in the wind speed direction comparison? How does that propagate into the uncertainty in the wake deflection analysis?

  We believe that some of the raised questions resulted from a bad structure of the section. Therefore, we modified Sect. 2.1 to introduce the measurement site only, and the instruments and measurements are then introduced in Sect. 2.2, separately. To answer the above questions here directly:

  - The target yaw offset was precomputed before the campaign based on an optimization with the Flow Redirection and Induction in Steady State (FLORIS) software from NREL as described in Fleming et al. (2019).
  - The wind directions were determined from the WindCube using the Doppler beam swinging technique (similar to the profiling lidar used in Lundquist et al., 2017).
  - The analytical models are compared with the measurements for the purpose of the validation of the models themselves and to evaluate the efficiency of the wake steering. One-to-one comparisons with the wake scanning Doppler lidars are made by computing the analytical models with the input variables measured by the WindCube and WindIris during each wake steering case.
  - The errors of the wind speed and the wind direction measurements are analyzed in section 3.1 (which was modified heavily to make it easier to follow and uniform in terms of used measurement data).
  - We assume that the RMSE between the WindCube and the WindIris as the error of the yaw angle, which is then propagated to the resulting error of the wake deflection using geometry. The resulting error is shown in Fig. 9b as errorbars.

  A reference to the section introducing the instruments and their measurements was added to section 2.1 (P3, L56-57). We added how the target yaw offset function was determined (P3, L62-63). The purpose of analytical models and how they are computed were added to Sect. 2.4 (P9, L190-191, L193-195, and P10, L203-206).

- Section 3.2 How were these wake deflection cases selected? Are you saying it is an analysis of all of the data from January to April? Please rewrite this section to help readers understand what you mean? What is a favorite in this context?
  'First, the wake deflection is verified for non-yawed control cases, where no wake deflection is expected. The distribution of the normalized wake deflection using the WindIris has a RMSE of 0:08 (Fig. 9a) and using the wind direction of the Wind-Cube with the nacelle position of T2 provides a RMSE of 0:07 (Fig. 9b). These errors agree with the RMSE of the yaw angle between 235 the two instruments (4sin(1:30_) =0:09) and both distributions have mean value that is not significantly different from zero. The consistency between the yaw angle errors and wake deflection distribution shows that the wake scanning and its spatial positioning were working well, and the absence of a bias shows that the alignment of the wake scanning lidar with the rotor axis is correct (the measured offset of 0:15_ during the installation was taken into account in the processing). Since we could not identify a clear favourite between the WindIris and the WindCube for the yaw angle, the average of both will be used for 240 the remainder of the article.'

  Both, the wake-steering cases and the control cases, are selected based on the criteria outlined in section 2.3.1. Briefly summarized:
    - The wake-steering cases require a northwestern wind direction with T3 downstream of T2 and active wake steering.
    - The control cases require a northeastern wind direction such that T2 will not yaw (limiting to northeaster directions also ensures that the inflow is undisturbed by other wind turbine wakes or topography as for the wake steering cases).

  There are 81 wake-steering cases and 76 control cases between 6 January 2019 and 9 April 2019 that fulfill the criteria of section 2.3.1. Their numbers are then further reduced by removing cases with unsuccessful wake center detections (due to insufficient SNR or bad Gaussian fits). A summary is presented in Table 1 below. We reworked Sect. 3.1, to use only the wake-steering cases and the control cases to be consistent with the remainder of the results section (it used all measurement data previously).

  With "no clear favorite", we wanted to express that the yaw angles measured by the WindIris and the WindCube compared well with each other and had no biases or any other apparent problem. Therefore, we had no reason to pick one over the other and instead used the average of both.

  An overview of the cases has been added at the beginning of the results section (P10, L212-213 and Table 1). Section 3.1 was modified to use data of the wake-steering cases and the control cases to make it consistent with remainder of the manuscript. Fig. 8 was modified to include the 3D scans of the control cases (analog to Fig. 9 for the wake-steering cases). It is specified in each figure caption which data is used (Fig. 5, 6 and 7). Section 3.2 was restructured and rephrased (P13, L243-251).

Table 1: Overview of wake-steering cases and control cases. From top to bottom: the number of 30-minute periods that met the requirements of Sect. 2.3.1, the number of cases with a sufficient SNR of the wake-scanning lidar, the number of cases with a successful detection of the wake center based on the correlation threshold (Sect. 2.3.3), and the number of cases for

which the model prediction of u_{mod} was possible (Sect. 2.4). The numbers outside of the brackets are the total number of cases, and the numbers inside the brackets are the 2D scans and 3D scans of the wake-scanning lidar, respectively.

	Wake-steering cases	Control cases
Cases based on Sect. 2.3.1	81 (36+45)	76 (27+45)
Cases with a sufficient SNR	56 (27+29)	66 (26+40)
Cases with a successful wake center detection	29 (16+13)	55 (21+34)
Cases with a prediction of u_{mod}	41 (19+22)	-

- Figure 7. Please add some quantitative comparison e.g. correlation coefficients, RMSE? How many measurements are included? Or excluded? How were they selected? It looks like about 30 measured points?

  Quantitative measures of the comparison have been added and the data is selected according to the criteria outlined in section 2.3.1, which is now stated at the beginning of the results section (see our response to the previous comment). The figure shows 29 data points for the wake-steering cases and 55 for the control cases.

  The RMSE and the correlation coefficient have been included to Fig. 7 and the caption states which data is used.

- Figure 8. This figure is probably key but again its very difficult to understand. Describe how you chose this case, describe how and where the measurements are located, describe how and where the models were implanted including the derivation of the freestream and its errors. Is tis a totally random case? Was it selected for some specific purpose?

  This case was chosen, because it has the largest yaw offset of the data set and therefore the largest magnitude of the wake deflection, which has two benefits: (i) the errors of the wake deflection are smallest relative to the wake deflection and (ii) the deflection is easy to visually observe. The models were computed from the inflow measurements of the WindCube and WindIris taken at the same time as the wake scanning as described in Sect. 2.4.

  We analyzed the influence of the measurement errors on the model error. The analytical models require γ, TI_{WI}, $u_{WC}(z)$, and the nacelle position of T2 from the SCADA data as input. In Sect. 3.1., the RMSE for γ and u_{WC} were determined as 1.42° and 0.42 m/s, respectively. We assume that the nacelle position from the SCADA data is virtually free of errors based on agreement with the position of hard targets in the scan field of the wake-scanning lidar. We could not do a validation for TI_{WI} and assume an accuracy of 0.015 as given in the manufacturer specifications instead. We quantified the error propagation by varying the model input based on the measurement errors for all investigated wake-steering cases. The errors resulting from TI_{WC} and γ led to uncertainties of 20 kW and 6 kW, respectively. The error resulting from u_{WC} resulted in the largest uncertainty with 61 kW.

  A detailed description of the example case was added to the manuscript text (P13, L252-260). After the restructuring section 3.2, the example case is now shown in Fig. 9a.

- Can you start by laying out the various cases in a table? Are there are examples, wake steering cases and the complete data set. Are there more? Like the wide case and the narrow case? It is difficult to follow and make comparisons. All of the comparisons should be in a table with the model results to allow a better evaluation? So for example, how does Table 2 compare with Table 1?

We added a table with an overview of the cases at the beginning of the results section. In addition, we made the usage of the measurement data uniform by modifying Sect. 3.1. Now, the results only use the wake-steering cases and the control cases (and examples chosen from the wake-steering cases).
Only Section 3.4 deviates from this structure as explained at the beginning of its subsections (which includes Fig. 12 and Table 2). In Sect. 3.4.2, we compare a period with wake steering to a period without wake steering, which is not possible based on the definition of the wake-steering cases. In Sect. 3.4.2, we only subdivide the wake-steering cases based on the wind direction to illustrate that the wake steering setup was suboptimal.

An overview of the used measurement data was added at the beginning of the results section (P10, L212-213 and Table 1). Section 3.1 was reworked overall to make usage of the measurement data uniform and easier to follow. The captions of Figures 5, 6, 10, 11, 13, and 14 as well as Table 3 were updated to state which date they are using.

- In the conclusions please evaluate this study in terms of: 1) Measurement errors vs model errors 2) Magnitude of wake steering vs errors 3) Comparison with other data sets – what is the overall assessment in terms of the viability of wake steering.

Regarding the model errors and the magnitude of the wake steering effect:
  - The effect of wake steering on the power is now also estimated from the wake-scanning Doppler lidar independent from the model (Fig. 14a and Table 3). These results show the same behavior as the analytical model. Especially, a reduced wake steering success for wind directions outside a narrow wind direction range between 325° and 335° is consistent with results of the analytical model.
  - The effect of wake steering depends mainly on the deflection of the wake, which the model can predict fairly well. The model errors for the power prediction also includes contributions from the power coefficient and nonstationary conditions, that do not directly enter into the model-to-model comparison from which the wake steering is evaluated. The shortcomings of the power coefficient for a partially waked turbine is responsible for a third of the model error. We reworked Sect. 3.3.2 to better distinguish the various error sources.

In summary, the found model errors do include contributions from the measurement errors, but they do not prevent the evaluation of the wake-steering setup. We believe that the identified problem areas of the model are important conclusions themselves. E.g., a study by Walker et al. (2016) does not list the power coefficient as an important error source in a model validation for wake losses.

Another important conclusion of the paper is that the implemented wake steering was performing suboptimal due to a bias of the wind direction perceived by the wind turbine once it had a yaw offset among other issues. This point is better highlighted in the conclusions, now. We believe that our study is not suited to provide an overall assessment of the viability of wake steering for two reasons: (i) as mentioned above, the investigated wake-steering setup was

not working as intended, and (ii) the investigated wake-steering cases only cover a limited range of atmospheric conditions (e.g., the employed methods limited the analysis to stationary conditions). However, we found that the wake steering improved the power output in some cases despite the issues with the wind vane on top of the nacelle.
This conclusion is in line with other studies. For example Vollmer et al. (2016) already concluded that the wake steering success is sensitive to the wind direction input. Simley (2020) came to similar conclusions based on a SCADA data driven approach, but without the wake-scanning lidar showing the wake position relative to the downstream turbine.

The conclusions were modified to and place a stronger emphasis on the suboptimal wake-steering setup and possible remedies (P24, L376-387). The influence of measurement conditions and measurement errors on the model errors is included to the conclusions (lines P24, L372-375).

- Please provide a data access statement.

A data statement is now included in the manuscript (P24, L394).

- Please check for typos.

A lot of typos were corrected throughout the manuscript based on feedback of a native English speaker. The changes are too numerous to be listed fully.

Literature

Barthelmie RJ, Pryor SC, Frandsen ST, Hansen KS, Schepers J, Rados K, Schlez W, Neubert A, Jensen L, Neckelmann S (2010) Quantifying the impact of wind turbine wakes on power output at offshore wind farms. J Atmos OceanTechnol 27(8):1302–1317

Lundquist, J. K.,Wilczak, J. M., Ashton, R., Bianco, L., Brewer,W. A., Choukulkar, A., Clifton, A., Debnath, M., Delgado, R., Friedrich, K., Gunter, S., Hamidi, A., Iungo, G. V., Kaushik, A., Kosovi´c, B., Langan, P., Lass, A., Lavin, E., Lee, J. C.-Y., McCaffrey, K. L., Newsom, R. K., Noone, D. C., Oncley, S. P., Quelet, P. T., Sandberg, S. P., Schroeder, J. L., Shaw, W. J., Sparling, L., Martin, C. S., Pe, A. S., Strobach, E., Tay, K., Vanderwende, B. J.,Weickmann, A.,Wolfe, D., andWorsnop, R.: Assessing State-of-the-Art Capabilities for Probing the Atmospheric Boundary Layer: The XPIA Field Campaign, B. Am. Meteorol. Soc., 98, 289–314, https://doi.org/10.1175/BAMS-D-15-00151.1, https://doi.org/10.1175/BAMS-D-15-00151.1, 2017.

Porté-Agel F, Wu YT, Chen CH (2013) A numerical study of the effects of wind direction on turbine wakes and power losses in a large wind farm. Energies 6(10):5297–5313

Fleming P, King J, Dykes K, Simley E, Roadman J, Scholbrock A, Murphy P, Lundquist J K, Moriarty P, Fleming K, van Dam J, Bay C, Mudafort R, Lopez H, Skopek J, Scott M, Ryan B, Guernsey C and Brake D 2019 Wind Energy Science 4 273-285.

Carbajo Fuertes, F.; Markfort, C.D.; Porté-Agel, F. Wind Turbine Wake Characterization with Nacelle-Mounted Wind Lidars for Analytical Wake Model Validation. Remote Sens. 2018, 10, 668.

Lidar measurements of yawed wind turbine wakes: characterisation and validation of analytical models

Peter Brugger[1], Mithu Debnath[2], Andrew Scholbrock[2], Paul Fleming[2], Patrick Moriarty[2], Eric Simley[2], David Jager[2], Mark Murphy[2], Haohua Zong[1], and Fernando Porté-Agel[1]

[1]Wind Engineering and Renewable Energy Laboratory (WiRE), École Polytechnique Fedérale de Lausanne (EPFL), 1015 Lausanne, Switzerland

[2]National Renewable Energy Laboratory (NREL), 15013 Denver West Parkway, Golden, Colorado, 80401, USA

Correspondence: Peter Brugger (peter.brugger@epfl.ch)

Abstract. Wake measurements of a scanning Doppler lidar mounted on the nacelle of a ~~yawed~~ full-scale wind turbine ~~are~~ during a wake-steering experiment were used for the ~~characterization~~ characterisation of the wake flow, the evaluation of the wake-steering setup, and the validation of analytical wake models. Inflow scanning Doppler lidars, a meteorological mast~~and the data~~ , and the supervisory control and data acquisition (SCADA) system of the wind turbine ~~control system complemented the set-up. Results~~ complemented the setup. Results from the wake-scanning Doppler lidar showed an increase of the wake deflection with the yaw angle~~that agreed with two of the three compared models. For yawed cases, the predicted power of a waked downwind turbine estimated by the two previously successful models had an error of 17% and 24% compared to the SCADA data and 12% and 13% compared to the power estimated from the Doppler lidar measurements. Shortcomings of the method to compute the power coefficient in an inhomogeneous wind field are likely the reason for disagreement between estimates using the Doppler lidar data versus SCADA data. Further, it was found that some wake steering cases were detrimental to the power output due to errors~~ , and that the wake deflection was not in all cases beneficial for the power output of a downstream turbine due to a bias of the inflow wind direction perceived by the yawed wind turbine and the wake steering design implemented. ~~Lastly, it was observed that the spanwise cross-section~~ Both observations could be reproduced with an analytical model that was initialized with the inflow measurements. Error propagation from the inflow measurements that were used as model input, and the power coefficient of a waked wind turbine contributed significantly to the model uncertainty. Lastly, the spanwise cross section of the wake ~~is~~ was strongly affected by wind veer, masking the ~~kidney-shaped wake cross-sections observed from wind-tunnel experiments and numerical simulations~~effects of the yawed wind turbine on the wake cross sections.

1 Introduction

Wind turbines in wind farms can influence other turbines downstream and impact their performance. The interaction of the turbine rotor blades and the wind field creates a spatial volume of reduced wind speed and increased turbulence levels downstream of a wind turbine that can extend for several rotor diameters (Vermeer et al., 2003). This region is called the wake and affects downwind turbines negatively by decreasing power production and increasing fatigue loads (Thomsen and Sørensen, 1999). The spatial proximity of wind turbines in a wind farm, and the wake effects on downwind turbines~~are an important source~~ , are important sources of power losses ~~(Barthelmie et al., 2010).~~ (Barthelmie et al., 2010). The magnitude of the power loss depends on wind direction, turbine spacing, wind speed, turbulence levels, and atmospheric stability (Stevens and Meneveau, 2017). In case of a fully waked wind turbine losses around 40% compared to a wind turbine in the free flow have been observed (Barthelmie et al., 2010; Simley et al., 2020).

Mitigating these wake effects on downwind turbines is an ongoing focus of research. Strategies that have been proposed are adjusting the blade pitch angle and the generator torque (Bitar and Seiler, 2013), counter-rotating rows of wind turbines in wind farms (Vasel-Be-Hagh and Archer, 2017), optimizing the placement of the turbines within the wind farm based on terrain and wind climate ~~(e.g. Shakoor et al., 2016; Kuo et al., 2016)~~(e.g., Shakoor et al., 2016; Kuo et al., 2016), or deflecting the wake away from the downwind turbine by introducing a yaw offset to the upwind turbine (Medici and Dahlberg, 2003). The latter approach, called wake steering or active yaw control, is the focus of this paper. It utilizes the thrust force that the rotor imposes on the flow and, by offsetting the rotor from the flow direction, a transverse component of the thrust force is generated that displaces the wake from the line of the wind direction with the goal to deflect it away from the downwind turbine. While the power production of the yawed turbine is reduced, this loss is potentially overcompensated for by the power gains of the downwind turbine (Bastankhah and Porté-Agel, 2015), and the strategy can be extended to a full wind farm (Gebraad et al., 2016). Wind-tunnel studies of wake steering showed an increase in power for the combined upstream-downstream turbine pair between 3.5% and 11% depending on inflow turbulence level and turbine separation distance (Bartl et al., 2018) and a field test at two commercial wind turbines showed an increase by 4% (Fleming et al., 2019).

Analytical models describe the wake of a yawed wind turbine based on a set of turbine and inflow parameters (Jiménez et al., 2009; Bastankhah and Porté-Agel, 2016; Qian and Ishihara, 2018). These models are computationally cheap compared to numerical simulations and therefore can be used to find a set of yaw angles that maximizes the power output (Gebraad et al., 2016; Fleming et al., 2019). Validation of the analytical models for yawed wind turbine wakes and studies on the effectiveness of the wake steering have been done with wind tunnel experiments ~~(e.g. Bastankhah and Porté-Agel, 2016)~~ (e.g., Bastankhah and Porté-Agel, 2016) and numerical simulations ~~(e.g. Vollmer et al., 2016)~~(e.g., Vollmer et al., 2016). However, studies of yawed wind turbines using field data are rare: Fleming et al. (2017a) and Annoni et al. (2018) analysed the wake deflection, the wake recovery, and the power output for an isolated yawed turbine; Fleming et al. (2017b) investigated the effects of wake steering on the power production for a yawed upwind and a waked downwind ~~turbines at an offshore-site; and~~ turbine at a land-based site; Bromm et al. (2018) investigated the wake deflection of a yawed turbine with remote-sensing instruments with detailed error analysis; most recently Simley et al. (2020) investigated the influence of the wind direction variability on the achieved yaw offsets and power gains based on the supervisory control and data acquisition (SCADA) data.

In this paper, field measurements, including inflow and wake measurements as well as ~~wind turbine control system~~ SCADA data from a ~~wake steering~~ wake-steering upwind turbine and a waked downwind turbine, are used to: (i) ~~characterize~~ characterise the wake flow in terms of deflection, velocity deficit, and width, (ii) ~~to~~ validate the wake deflection and power predicted from analytical models with the field measurements, and (iii) ~~to analyse the performance of the~~ evaluate the wake-steering ~~set-up~~ setup implemented at this site.

2 Methods

This section introduces the measurement site, the instruments, the analytical models, and the data processing used to obtain the results. Indices are used to distinguish quantities measured by different instruments~~(see appendix 1 for an overview)~~.

2.1 Research site and measurement setup

The measurement site is a large wind farm in northeast Colorado, United States. Measurements were conducted at an isolated cluster of five turbines at the ~~north-western~~ northwestern edge of the wind farm from 23 December 2018 until 06 May 2019 with the ~~set-up~~ setup shown in Fig. 1. The area north of the turbines is flat grassland, and to the south and ~~south-east~~ southeast is a downward terrain step of ~~approx.~~ approximately 150 m followed by flat grassland. The ~~measurement set-up consisted of an WindCube Doppler lidar and a meteorological mast that recorded vertical profiles of the wind speed and wind direction. A Stream Line Doppler lidar scanning the wake and a WindIris Doppler lidar scanning the inflow were installed on the nacelle of turbine 2 (T2). A thrid wake scanning Doppler lidar was installed on the nacelle of turbine (T3), but its data is not used in this study.Further, the SCADA data of T2 and T3 was provided by the wind park operator~~instruments measuring the inflow and the wake are introduced in Sect. 2.2. This article focuses on conditions with northern wind directions with flat grassland upwind and no structures or turbines affecting the inflow.

The wind turbines were of the type 1.5~~SLE~~ sle from General Electric Energy with active blade pitch control and a rated capacity of ~~1500~~1,500 kW. Their hub height, z_{hub}, is 80 m, and the rotor diameter D is 77 m. The SCADA data of T2 and T3 were provided by the wind park operator. T2 was equipped with a yaw controller to introduce a wind speed dependent yaw offset for wind direction between 324° and 348° to deflect the wake from T3 (Fig. 2a). The target yaw offset was precomputed based on an optimization with an engineering model of wake steering as described in Fleming et al. (2019). A negative yaw offset is a counterclockwise rotation of the nacelle viewed from above. The power curve and pitch control of T2 are shown in Fig. 2b and Fig. 2d, and for T3 in Fig. 2c and Fig. 2e. In absence of manufacturer information or measurement data for the thrust coefficient, and due to the similarity of the thrust coefficient for most commercial wind turbines, the assumed thrust coefficient curve of the wind turbine follows the ensemble average shown in Fig. 2d. For a yawed turbine, the thrust coefficient is adapted with $\widetilde{C}_T = C_T \cos^{1.5}\gamma$ (Bastankhah and Porté-Agel, 2017), and the power coefficient is modified with $\widetilde{C}_P = C_P \cos^3\gamma$ (Adaramola and Krogstad, 2011), which includes the reduction of the rotor swept area. The readings of the nacelle position in the SCADA data of T2 were incremented by $4°$ on 17 January 2019 without affecting the true nacelle position to remove a bias between the ~~the~~ wind direction perceived by T2 and the WindCube. If the nacelle position of T2 is used to compute the position of T3 within the field of view of the ~~wake scanning lidar~~wake-scanning lidar, this manipulation is reversed.

2.2 Measurement instruments

The instruments for the inflow and the wake measurements are introduced.

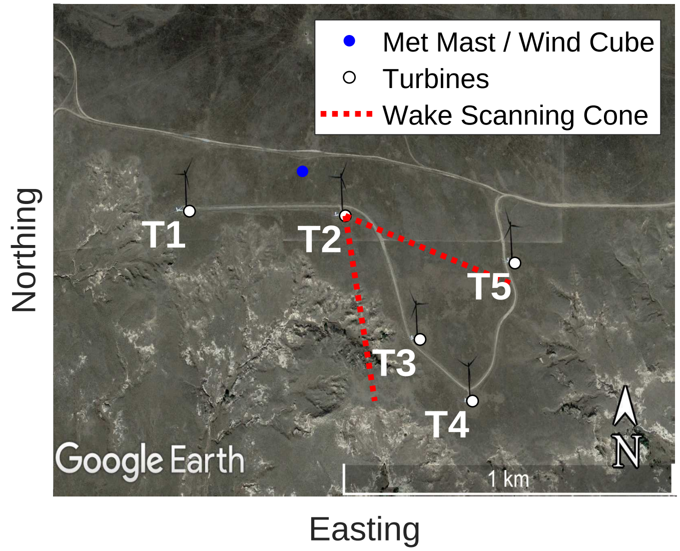

Figure 1. Overview of the measurement site and ~~set-up~~setup. Shown in white are the five turbines of the local cluster with the remainder of the wind park to the east. Turbine 2 (T2) was programmed to introduce a yaw offset, if turbine 3 (T3) was downwind. The distance between T2 and T3 is ~~approx.~~ approximately 390 m. T2 had two Doppler lidars installed on the nacelle to scan the inflow and the wake (Sect. 2.2.2 and 2.2.4). Shown in red is the scanning cone of the ~~wake scanning~~ wake-scanning Doppler lidar for a case with the wind direction aligned with the direction to T3 and a yaw angle of 20°. Shown in blue is the location of the meteorological mast and the Wind Cube (Sect. 2.2.3 and 2.2.1).

2.2.1 WindCube

A ~~WindCube~~ WindCube-V2 profiling Doppler lidar (~~version 2,~~ manufactured by Leosphere and NRG Systems, Inc.) was located ~~north~~ northwest of T2 and measured vertical profiles of the wind speed and the wind direction of the inflow (Fig.1). The lidar uses a laser wavelength of 1.54 μm and internally computes the wind speed (U_{WC}) and wind direction (dir_{WC}) from a ~~PPI~~ plan position indicator (PPI) scan with an azimuth step of 90° and an elevation angle of 62° followed by a vertical beam with the Doppler beam swinging technique assuming horizontal homogeneity (similar to the lidar in Lundquist et al. (2017)). The measurement data was filtered with a signal-to-noise ratio (SNR) threshold of ~~−19 dB~~ −22 dB. The WindCube was ~~set-up~~ setup to provide the vertical profiles from 40 m a.g.l. to 260 m a.g.l. with a height resolution of 20 m and ~~an averaging time~~ a sampling frequency of 1 ~~minute~~Hz. The WindCube data is available from 06 January 2019 until 09 March 2019. Further, the yaw angle (γ_{WC}) can be computed from the difference between the wind direction at hub height and the nacelle position of the T2.

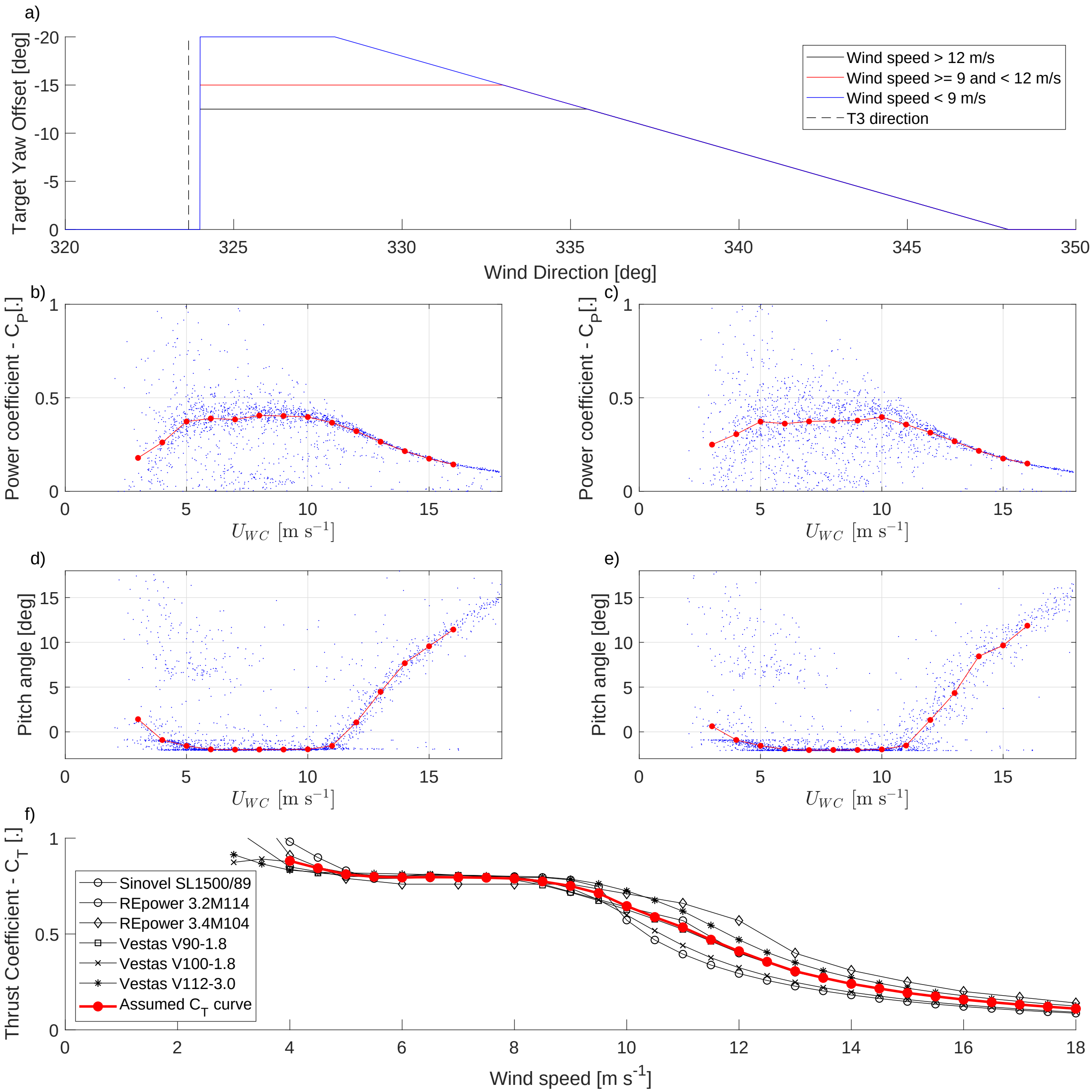

Figure 2. Characteristics of the wind turbines used ~~for~~ in the ~~wake steering test~~wake-steering experiment. The top panel (a) shows the target yaw offset as a function of the wind speed and wind direction for T2. Panels b) and d) show the 30-minute mean values (blue) and bin average (red) of the power coefficient and the blade pitch angle ~~of~~ from the ~~blades~~ SCADA data of T2 as a function of the wind speed ~~for T2 with~~ measured by the ~~SCADA data shown as blue dots and the bin averages in red~~WindCube (Sect. 2.2.1). Panels c) and e) show the same for T3. Data from 6 January until 9 April 2019 is used in consistency with the results presented in Sect. 3. The bottom panel (f) shows in black the thrust coefficient curves of six wind turbines from manufacturer data (first compiled by Abdulrahman (2017)) and in red the ensemble average assumed as C_T curve for T2.

2.2.2 WindIris

A WindIris Doppler lidar (manufactured by Avent Lidar Technology) was mounted on the nacelle of T2 scanning the inflow. The WindIris uses a ~~4 beam~~ four-beam geometry with measurements at $\pm 15°$ from the rotor axis in ~~horizontal and $\pm 5°$~~ the horizontal direction and $\pm 12.5°$ in the vertical direction. The WindIris provides the wind direction relative to the rotor axis (γ_{WI}), the wind speed (U_{WI}), and the longitudinal turbulence intensity (TI_{WI}) for an upwind distance of 50 m to 200 m from the turbine and heights of 45 m a.g.l. to 125 m a.g.l. Its measurements are within the induction zone of the turbine, and only vertically averaged measurements from ~~a~~ an upwind distance of 90 m are used as a compromise between good data availability and a large upwind distance. The WindIris had problems that led to data loss during the campaign, which limits data availability to 12, 16, and 19 January and a long period from ~~the~~ 24 January 2019 until ~~the~~ 07 April 2019.

2.2.3 Meteorological Mast

A meteorological mast was located ~~north-west~~ northwest of T2 next to the WindCube. The wind direction from the wind vanes at 38 m a.g.l. ($dir_{MM,38m}$) and 56 m a.g.l. ($dir_{MM,56m}$), the wind speed of the ultrasonic anemometer at 50 m a.g.l. (U_{Sonic}), and the wind speed of the cup anemometer at 60 m. a.g.l. (U_{MM}) will be used. The wind vanes had an alignment issue until the week of 11 February 2019, when they were replaced with freshly calibrated units, and the cup anemometer had periods of suspicious measurements that might be connected to icing of the instrument. Further, the measurement data is not available for a five periods during the campaign. For those reasons, the wind measurements from meteorological mast are only used for validation of the WindCube. Further, the meteorological mast measured air temperature and air pressure near the surface from which the density of dry air ρ_{MM} is computed.

2.2.4 Stream Line

A Stream Line Doppler lidar (manufactured by Halo Photonics Ltd.) was mounted on the nacelle of T2, scanning the wake downwind of the turbine. It performed an hourly scan schedule consisting of 2D and 3D scans of the wind field downwind. The 2D scans were horizontal swipes at an elevation of $0°$ covering an azimuth range from $160°$ to $220°$ with an azimuth step of $1.5°$ (Fig. 3a), which were repeated 53 times back and forth within a 28-minute period. The 3D scans consisted of PPI swipes at 9 elevation angles, which were repeated between 20 and 22 times within a 31-minute period. The 3D scan pattern was iterated throughout the campaign with changes to the covered azimuth range and positions of the elevation levels (compare Fig. 3b and 3c). These changes were made to capture the wake at short downwind distances, but have little effect on the measurements of the wake flow at the position of the downwind turbine. Further, other scan patterns were introduced to the scan schedule during the campaign, but those are not used in this study. The ~~StreamLine~~ Stream Line system had an azimuth misalignment from the rotor axis of $-0.15°$ after installation on the nacelle. Levelling of the instrument is affected by tower movements, but their effects on the beam positions are mitigated by a grid-based ~~post-processing~~ post processing of the measurement data introduced in the following section.

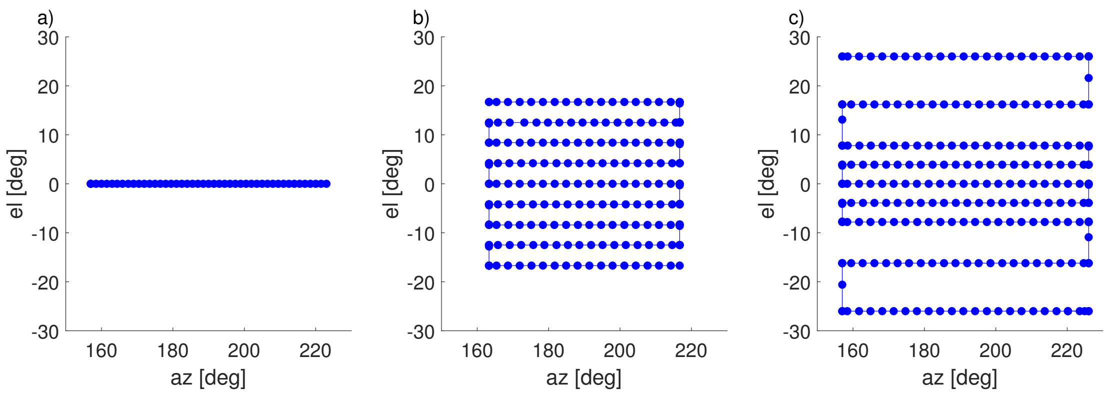

Figure 3. The scan pattern of the 2D (a) and the 3D scans with ~~equal~~ equally spaced elevation levels (b), and elevation levels with larger spacing at the top and bottom (c). The path of the scanner is shown as a blue line with measurement points indicated as blue points.

2.3 Data processing

The processing of the measurement data is introduced in the order in which it was done to obtain the results.

2.3.1 Inflow measurements and data selection

The 10-minute and 30-minute mean values and standard deviations of the wind speed, wind direction, and yaw angle were computed from the data of the WindCube, WindIris, meteorological mast, and SCADA data. A filter was used to identify suitable intervals for further processing of the ~~wake scanning~~ wake-scanning lidar. The filter criteria are as follows:

- Data ~~is~~ are available for the WindCube, the WindIris, and the SCADA data of T2 and T3.
- Wind speed from the WindCube and WindIris is between $4\ \mathrm{m\ s^{-1}}$ and $15\ \mathrm{m\ s^{-1}}$.
- Neither T2 nor T3 had a downtime, and the rotor was turning.
- The 10-minute period comprising a 30-minute period had changes of less than $3\ \mathrm{m\ s^{-1}}$ for the wind speed ~~,~~ and less than $5°$ for the wind direction.

Further, the 30-minute periods had to satisfy one of the two following conditions to be classified either as a ~~wake steering~~ wake-steering case or a control case:

- ~~Wake steering cases: north-western~~ Wake-steering cases: northwestern inflow with the WindCube wind direction between $320°$ and $350°$, active yaw control of T2 (compare Fig. 2a), and the mean yaw angle between $3°$ and $30°$ for both WindIris and WindCube.
- Control cases: north to ~~north-eastern~~ northeastern inflow with the WindCube wind direction between $0°$ and $75°$ and the yaw angle between $-3°$ and $3°$ for both WindIris and WindCube.

The processing of the ~~wake scanning~~ wake-scanning Stream Line Doppler lidar described in the next section was carried out for periods that satisfied the above filtering criteria. Periods were rejected at later stages if the measurements of the Stream Line system were not available or the SNR filter rejected measurements in the investigated scan area. Because the selection of suitable periods described here is based on 30-minute periods, but the 2D and the 3D scans of the Stream Line Doppler lidar were 28 and 31 minutes long, respectively, the final inflow parameters used for the results were ~~re-computed~~ recomputed for the precise scan durations at a later stage.

2.3.2 Processing of ~~wake scanning~~ wake-scanning Doppler lidar data

For the suitable periods identified in the previous section, the data of the ~~wake scanning~~ wake-scanning Stream Line system was processed along the following steps:

- A ~~signal-to-noise ratio (SNR)~~ SNR filter with a threshold of -17 dB was applied to remove ~~low quality~~ low-quality data points. If the mean SNR at hub height was too low at a distance of $4D$, the scan was rejected altogether (e.g.~~periods with aerosol free~~ , periods with aerosol-free air or fog).

- The azimuth angle of each lidar beam was adjusted so that the measurements were fixed in space relative to the ground by removing changes of the nacelle position recorded in the SCADA data. The transformation is given by:

  $$az_{wsl,i} = az_{wsl,i} + (az_{SC,i} - \overline{az_{SC}}) \qquad (1)$$

  with $az_{wsl,i}$ the azimuth angle of the i-th beam during the scan, $az_{SC,i}$ is the nacelle position of T2 at the time of the measurement, and $\overline{az_{SC}}$ the angular mean nacelle position for the scan duration. A rejection of periods with excessive nacelle position changes was not necessary ~~, because the stationarity~~ because the stationariness criterion of the wind direction in the previous section already removed periods with large changes of the nacelle position.

- The measurements were rotated into the mean wind direction such that it aligned with $az = 180°$ of the ~~wake scanning lidar with~~wake-scanning lidar with:

  $$az_{wsl,i} = az_{wsl,i} + \gamma. \qquad (2)$$

- The radial velocity measured by the Doppler lidar was transformed to the longitudinal velocity based on elevation and azimuth angles, sorted into a regular spherical coordinate system, and interpolated on a Cartesian coordinate system with 10 m resolution. These procedures are described in Fuertes et al. (2018) for the 2D scans and in Brugger et al. (2019) for the 3D scans.

The above steps provided the longitudinal mean velocity field $u_{2D}(x,y)$ and $u_{3D}(x,y,z)$ in a Cartesian right-hand system with origin at the nacelle of T2, and the x-axis pointing in the wind direction and the z-axis ~~upwards~~pointing upward. The corresponding velocity deficits are then given by:

$$\Delta u_{2D}(x,y) = u_{WC}(80\ \mathrm{m}) - \mathrm{u_{2D}(x,y)} \qquad (3)$$

and

$$\Delta u_{3D}(x,y,z) = u_{WC}(z) - u_{3D}(x,y,z) \tag{4}$$

with $u_{WC}(z)$ interpolated to the grid heights.

2.3.3 Wake ~~center~~ deflection from the wake-scanning Doppler lidar

The wake was characterized by fitting a Gaussian function given by:

$$g(\delta,\sigma,C) = C\exp\left(\frac{(y-\delta)^2}{\sigma^2}\right) \tag{5}$$

to $\Delta\overline{u}_{2D}(x,y)$ and $\Delta\overline{u}_{3D}(x,y,z_{hub})$ at each downwind distance. The fit used a Gaussian weighting function with a width of 1.5σ. The position of the peak given by $\delta(x)$ is equivalent to the wake deflection ~~,~~ because the coordinate system was rotated into the wind direction (Eq. 2). To remove cases where the Gaussian fit was influenced by the wakes or the hard targets of neighbouring turbines, and to ensure that only results within the far wake are used, the result was rejected if the correlation coefficient of the Gaussian fit and the measurement data ~~was~~ were below 0.99 at $x/D = 4$ (a visual verification showed that all instances of this problem were detected).

2.3.4 Power and rotor-averaged velocity from the Doppler lidars

The power of the upwind turbine (T2) was computed from the inflow measurements of the WindCube with the assumption that the inflow is horizontally homogeneous across the rotor area. It is then given by:

$$P_{WC} = \frac{1}{2}\rho_{mm}C_{P,T2}\cos^3\gamma\iint\limits_A u_{WC}^3(z)\,\mathrm{d}y\mathrm{d}z, \tag{6}$$

with the rotor area A defined by $\cancel{\sqrt{y^2+(z-z_{hub})^2} \leq 0.5D}$ $\sqrt{y^2+(z-z_{hub})^2} \leq 0.5D$, and $C_{P,T2}$ was interpolated from the power curve of T2 shown in Fig. 2 based on the $U_{WC}(z_{hub})$. For the downwind turbine (T3), the power was computed from the longitudinal velocity field of the ~~wake scanning~~ wake-scanning lidar by integration over the rotor area. It is given by:

$$P_{wsl} = \frac{1}{2}\rho_{mm}C_{P,T3}\iint\limits_A u_{3D}^3(4D,y,z)\,\mathrm{d}y\mathrm{d}z, \tag{7}$$

with $\sqrt{(y-y_{T3})^2+(z-z_{hub})^2} \leq 0.5D$ and y_{T3} the transverse position of the T3 in the coordinate system aligned with the wind direction. The integrals were approximated by sums according to the grid resolution of the measurement data. The power coefficient was interpolated from the power curve of T3 based on the average velocity across the rotor area for T3 ~~. The integrals were approximated by sums according to the grid resolution of the measurement data.~~ given by:

$$U_{wsl} = \overline{u_{3D}(4D,y,z)} \tag{8}$$

with $\sqrt{(y-y_{T3})^2+(z-z_{hub})^2} \leq 0.5D$ and the bar indicating a mean value. The power that T3 would have produced for a nonyawed T2, $P_{wsl,\gamma=0}$, is estimated from the wake-scanning lidar with Eq. (7) and $\sqrt{(y-y_{T3}+\delta(4D))^2+(z-z_{hub})^2} \leq 0.5D$

under the assumption that yawing effects primarily the spatial position of the wake and effects on the shape of the wake are minor.

2.4 Analytical Models

Three analytical models are compared with the field measurements ~~in this study~~for validation of the models themself and to investigate the efficency of the wake-steering setup. The analytical models were introduced by Jiménez et al. (2009), Bastankhah and Porté-Agel (2016), and Qian and Ishihara (2018), respectively, and their equations are presented in Appendix ~~2.~~ A. All three models use the longitudinal turbulence intensity of the WindIris, the average yaw angle of the WindIris and the WindCube, ~~the yaw angle,~~ and the thrust coefficient as input variables and predict the longitudinal velocity deficit field $\Delta u_{mod}(x,y,z)$ of the wake. The thrust coefficient is interpolated from the assumed thrust curve in Fig. 2f with the wind speed of the WindCube. The models are computed for each investigated 30-minute period separately with the same 10 m resolution Cartesian coordinate system as the velocity fields of the ~~wake scanning~~ wake-scanning lidar for consistency. Together with the inflow measurements of the WindCube, the longitudinal velocity field is computed with:

$$u_{mod}(x,y,z) = \Delta u_{mod}(x,y,z) + u_{WC}(z), \tag{9}$$

where $u_{WC}(z)$ is interpolated to the grid levels. The model prediction for the rotor-averaged velocity and the turbine power of T3, P_{mod} and U_{mod}, is then computed from the model analogous to Eq. (7) and Eq. (8), but with the predicted longitudinal velocity field of the analytical model instead of the velocity field from the lidar measurements. The power of T3 for a hypothetically nonyawed T3, $P_{mod,\gamma=0}$, is estimated by computing the model with $\gamma = 0°$. However, $u_{mod}(x,y,z)$ cannot be evaluated at downstream distances shorter than the predicted onset of the far wake. This can become a problem with the short turbine spacing of the measurement site for cases with very low turbulence intensities of the inflow and these cases will be discarded from the results where appropriate.

3 Results and Discussion

The ~~time frame of analysis is~~ analysed time frame is from 6 January 2019 until 9 April 2019 ~~, because~~because, outside of that time frame~~data of~~ , data of either the WindIris or the WindCube was missing. The synoptic conditions were characterized by the winter season with daily mean temperatures mostly between ~~−10 °C and 5 °~~ −10° C and 5° C. The main wind directions were ~~north-west and south-east~~ northwest and southeast with wind speeds up to 25 m s^{-1} (Fig. 4).

The results presented in the following are based on the wake-steering cases and the control cases as defined in Sect. 2.3.1 (with the exception Sect 3.4.1). Table 1 presents a summary of the available cases. Periods of clear air and snow or fog events ~~further reduced data availability of the remote sensing instruments~~reduced the SNR of the wake-scanning lidar and its data availability. Further, the detection of the wake deflection or the prediction of $u_{mod}(x,y,z)$ failed for some cases, which will be discarded where necessary.

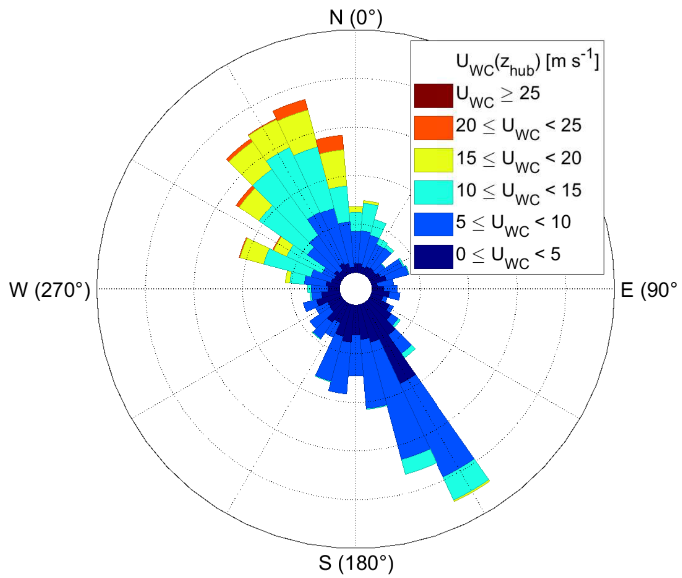

Figure 4. Wind rose based on the u_{WC} and dir_{WC} at hub height using the full data set from 6 January 2019 until ~~09~~ 9 April 2019. Software written by Daniel Pereira was used to create the wind rose (https://www.mathworks.com/matlabcentral/fileexchange/47248-wind-rose, MATLAB Central File Exchange, Retrieved 11 December 2019).

Table 1. Overview of wake-steering cases (middle column) and control cases (right column). From top to bottom: the number of 30-minute periods that met the requirements of Sect. 2.3.1, the number of cases with a sufficient SNR of the wake-scanning lidar, the number of cases with a successful detection of the wake center based on the correlation threshold (Sect. 2.3.3), and the number of cases for which the model prediction of $u_{mod}(x,y,z)$ was possible (Sect. 2.4). The numbers outside of the brackets are the total cases, and the numbers inside the brackets are the 2D scans and 3D scans of the wake-scanning lidar, respectively.

	wake-steering cases	control cases
Cases based on Sect. 2.3.1	81 (36 + 45)	76 (27 + 45)
Cases with a sufficient SNR	56 (27 + 29)	66 (26 + 40)
Cases with a successful wake center detection	29 (16 + 13)	55 (21 + 34)
Cases with a prediction of $u_{mod}(x,y,z)$	41 (19 + 22)	-

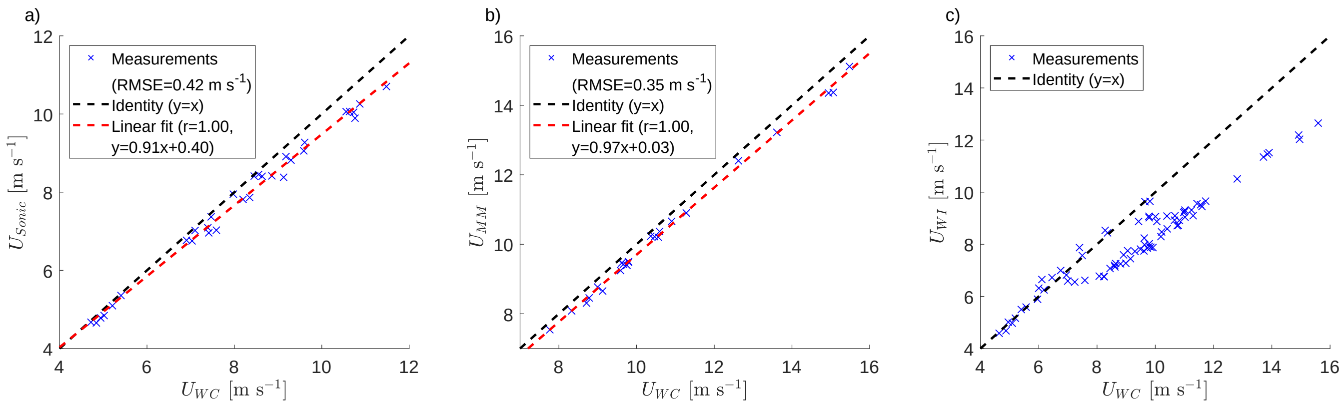

Figure 5. ~~Inter-comparison~~ Intercomparison of the inflow wind speed measurements between the ultrasonic anemometer at 50 m and the WindCube at 60 m (left panel, a), the meteorological mast at 60 m and the WindCube at 60 m (middle panel, b), and the WindIris and the WindCube at hub height (right panel, c) using the wake-steering and the control cases. Measurement data of the ultrasonic anemometer and the cup anemometer were not available for all cases. The black dashed line shows the identity $x = y$, and a linear fit is shown as a red dashed line together with the correlation coefficient r.

3.1 Inflow

The inflow measurements, especially of the yaw angle, are essential for the quality of the results presented in the following sections. Therefore, an ~~inter-comparison~~ intercomparison of the inflow measurements for wind speed, wind direction, and yaw angle will be presented~~first~~.

The wind speed from the WindCube, ultrasonic anemometer, cup anemometer, and WindIris are compared in Fig. ~~??. All available data during the analysis time frame is used for the comparison irrespective of the filtering criteria (Sect. 2.3.1).~~ 5. The WindCube shows good agreement to the ultrasonic anemometer with ~~correlation coefficient of 0.99, a slope near unity and a RMSE of 0.68 m s^{-1} (Fig. ??a). The underestimation at high wind speed~~ a slight underestimation by the ultrasonic anemometer at heigh wind speeds, which might be explained by the height difference ~~.~~ (Fig. 5a). The agreement between the WindCube and the cup anemometer is also good with ~~correlation coefficient of 0.98,~~ a slope near unity and a ~~RMSE of 1.00 m s^{-1}~~ small underestimation by the cup anemometer (Fig. ~~??~~5b). ~~However, here we removed two periods of data around the 07 February 2019 and 26 February 2019 were the cup anemometer showed consistently low wind speeds. Both periods coincide with very low temperatures according to the air temperature measurement at 2 m and icing of the cup anemometer might have played a role here. An underestimation at high wind speeds is not observed.~~ The WindCube and the WindIris show systematic deviations due to the induction zone of the wind turbine (Fig. ~~??~~5c). Based on this comparison, the wind speed of the WindCube will be used in the following ~~,~~ because it is available at hub height, not influenced by the induction zone, and compares well with the ultrasonic and cup anemometer.

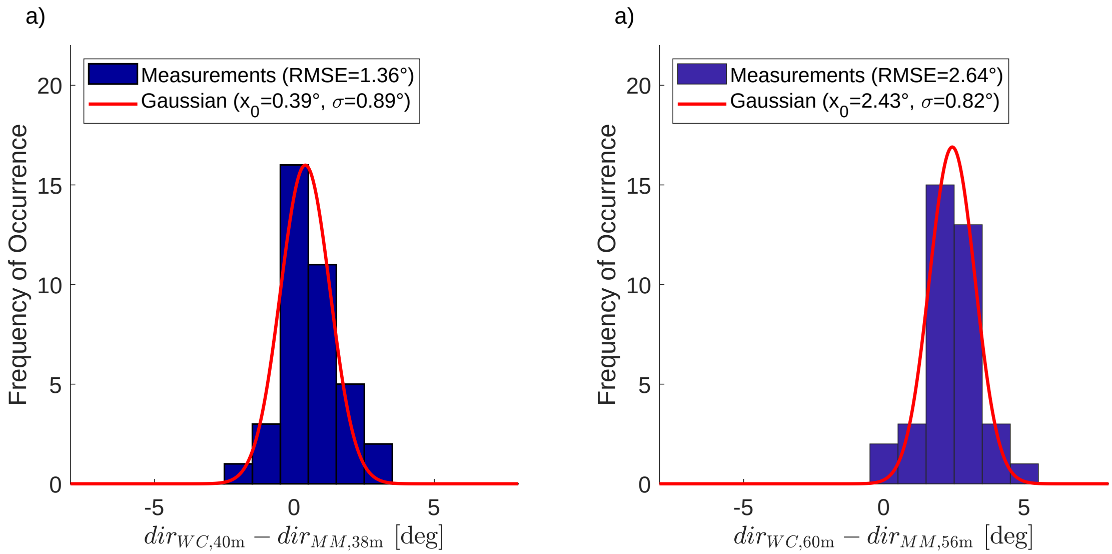

Figure 6. ~~Comparison~~ Histogram of the ~~inflow~~ wind direction ~~measurements from~~ difference between the WindCube and the meteorological mast for 40 m a.g.l. (left panel, a) and 60 m a.g.l. (right panel, b) using the wake steering and the control cases after 16 February ~~2019.~~ 2019 (the wind vanes on the meteorological mast were misaligned before 16 February 2019). The ~~black dashed~~ red line shows ~~the identity $x = y$ and~~ a ~~linear~~ Gaussian fit ~~is shown as a red dashed line. Black crosses are data points that were excluded from~~ to the ~~linear fit~~histogram.

The wind direction from the WindCube and the two wind vanes of the meteorological mast have ~~an~~ a large offset to each other until ~~the~~ a five day maintenance starting on 11 February ~~2019 after which the mast data is unavailable for five days due to maintenance. After the~~ 2019. Therefore, only the wake steering and the control cases after 16 ~~February~~ Feburary 2019 ~~,~~ ~~both heights agree with the WindCube~~ are used for the wind direction comparison (Fig. ~~??). As for the wind speed above, the filtering criteria are not applied here. The RMSE is 5.54°~~ 6). The RMSE of 1.36° for the lower wind vane and ~~6.25°~~ 2.64° for the upper wind vane ~~. The wind direction of the WindCube and the wind vane has a correlation coefficient of 1.00 and a slope near unity at both heights~~include contributions from a remaining bias between WindCube and wind vanes. If the bias is removed, the RMSE reduces to 1.23° and 1.61°, respectively. The findings for the yaw angle shown in the next paragraph suggest, that the WindCube has a correct north alignment. As for the wind speed, the WindCube will be used as reference for the wind direction ~~,~~ because it agrees ~~well~~ with meteorological mast after its maintenance, so it is presumably also correct before.

The yaw angle from the WindIris, the SCADA data, and the WindCube are compared (Fig. ~~??~~7). The ~~data filtering~~ data-filtering criteria of Sect. 2.3.1 were applied ~~here, but~~ without the yaw angle restriction for the control cases~~. This limitation to northern inflow directions for the comparison is due to the wakes of the neighbouring wind turbines affecting the comparison negatively for other inflow directions~~, because it would artificially reduce the measurement errors. For the ~~non-yawed~~ nonyawed control cases, ~~a RMSE of 1.82° was found between~~ the yaw angle of the SCADA data and the ~~WindIris. The Gaussian fit suggests~~ WindCube have a similar RMSE with the WindIris and a bias of less than 1° ~~between the instruments~~ (Fig. ~~??a). The WindCube~~

~~and the WindIris have a RMSE of $1.30°$ and a smaller bias than the SCADA data for the control cases (~~7a and Fig. ~~??~~7c). For the ~~wake steering~~ wake-steering cases, a large bias between the WindIris and the SCADA data can be seen for $\gamma < -5°$ (Fig. ~~??b) ,~~ 7b) that is not present between the WindCube and the WindIris (Fig. ~~??~~7d). ~~That observation suggests that yawing of the wind turbine affects the measurements of the wind vane on top of the nacelle. This view is supported by an increase~~ This is reflected in a doubling of the RMSE ~~to $2.10°$~~ between the WindIris and the SCADA data from the control cases to the wake-steering cases, while the RMSE between the WindCube and the WindIris ~~did only change slightlyto $1.32°$ for the wake steering cases~~increased only slightly. This observation suggests that yawing of the wind turbine affects the measurements of the wind vane on top of the nacelle.

3.2 Wake deflection

~~The deflection of the wake center from the downwind direction is investigated. The wake deflection is evaluated at a downwind distance of $x/D = 4$ to avoid the influence of hard targets or wakes of neighbouring turbines at larger distances and the near wake at smaller distances (Fig. ??).~~

~~First~~Before investigating the wake deflection caused by the wake steering, the wake deflection is verified for ~~non-yawed control cases ,~~ the nonyawed control cases where no wake deflection is expected ~~. The distribution of the normalized wake deflection using the WindIris has a RMSE of 0.08~~ (Fig.8). Based on the RMSE found for the yaw angle (Fig. 7c and Fig. 7d), the expected RMSE of the wake deflection should be between $4 \cdot \sin(1.16°) = 0.08$ and $4 \cdot \sin(1.42°) = 0.10$. This is the case for the for the WindIris (Fig. ~~??~~8a) and ~~using the wind direction of the WindCube with the nacelle position of T2 provides a RMSE of 0.07~~ the WindCube (Fig. ~~??~~8b). ~~These errors agree with the RMSE of the yaw angle between the two instruments ($4\sin(1.30°) = 0.09$) and~~ Further, both distributions have a mean value that is not significantly different from zero. The consistency between the yaw angle errors and the wake deflection distribution shows that the ~~wake scanning~~ wake-scanning and its spatial positioning were working well~~, and the~~ . The absence of a bias shows that the alignment of the ~~wake scanning~~ wake-scanning lidar with the rotor axis is correct (the measured offset of $0.15°$ during the installation was taken into account in the processing). ~~Since we could not identify a clear favourite between the~~ Because the yaw angle and the wake deflection provided by the WindIris and the WindCube ~~for~~ are of comparable quality, the yaw angle, ~~the average of both will be used for~~ γ, used in the remainder of the article will be the average of both.

~~The wake deflection for the wake steering cases~~

The deflection of the wake center from the downwind direction due to wake steering is investigated, next, starting with a discussion of the example case shown in Fig. 9a. This case was selected, because it has the largest yaw offset of all wake-steering cases, which makes the wake deflection easy to visually observe in the mean longitudinal velocity field. The wake center detection was successful around $x/D = 4$, but the non-Gaussian shape of the near wake and neighbouring wind turbine wakes led to problems at other downwind distances, which were detected and rejected with the correlation threshold (Sect. 2.3.3). The analytical models were computed from the inflow measurements taken at the same time as the exmaple case as described in Sect. 2.4 and are also shown in Fig. 9a. The Bastankhah and Porté-Agel (2016) model and Qian and Ishihara (2018) model show visually good agreement with the observed wake deflection, but the Jiménez et al. (2009)

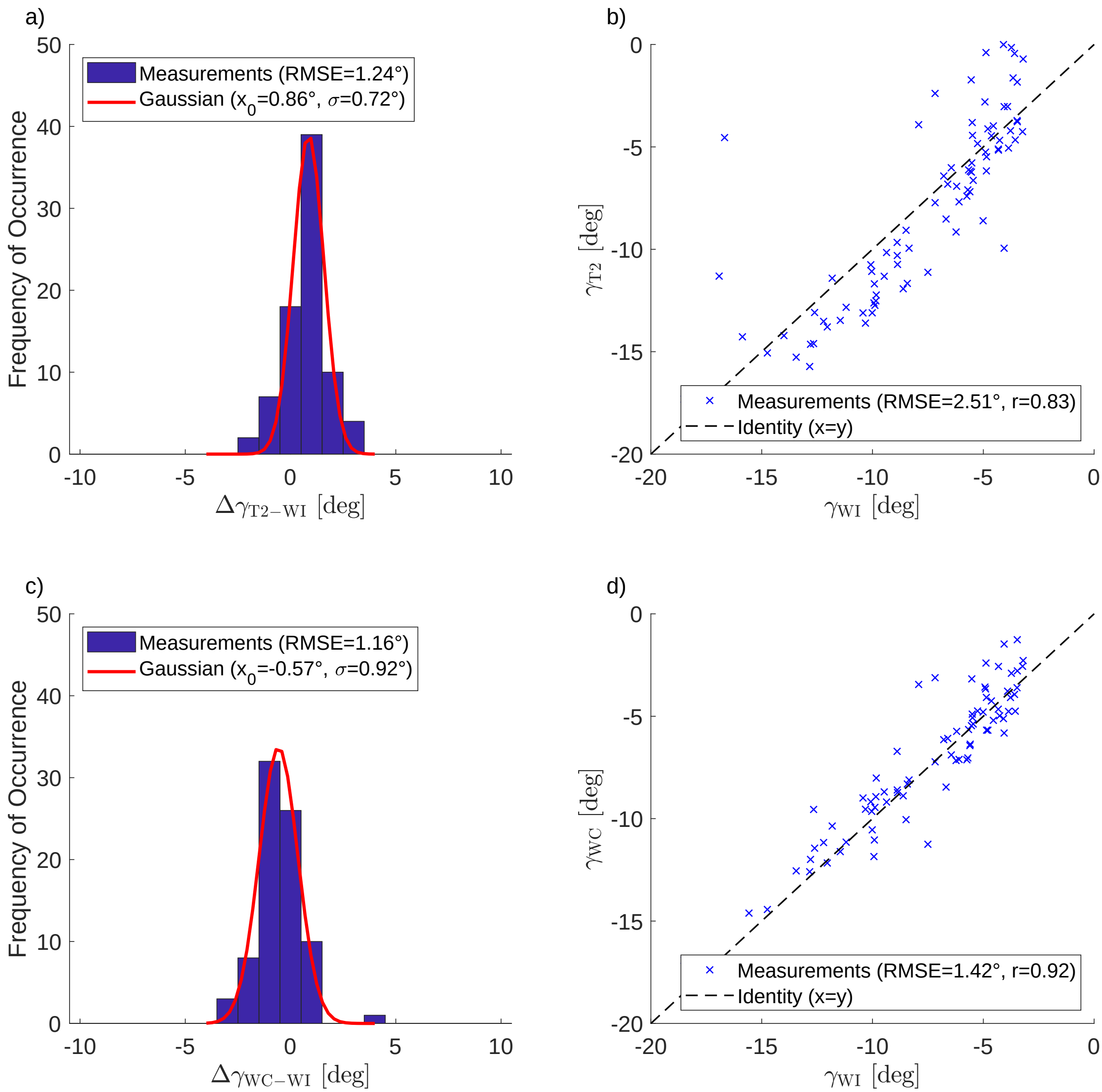

Figure 7. ~~Inter-comparison~~ Intercomparison of the yaw angle measurements. The top left panel (a) shows a histogram of the yaw angle difference between the WindIris and the SCADA data of T2 for the control cases. The top right panel (b) shows the yaw angle from the SCADA data of T2 and the WindIris for ~~wake steering~~ wake-steering cases. The bottom left panel (c) shows a histogram of the yaw angle difference between the WindCube and the WindIris for the control cases. The bottom right panel (d) shows the yaw angle from the SCADA data of T2 and the WindIris for ~~wake steering~~ wake-steering cases. The red line shows a Gaussian fit to the histogram, and the black dashed line is the identity. The data was filtered according to Sect. 2.3.1, but for panel (a) and (c) the yaw angle limitation was omitted.

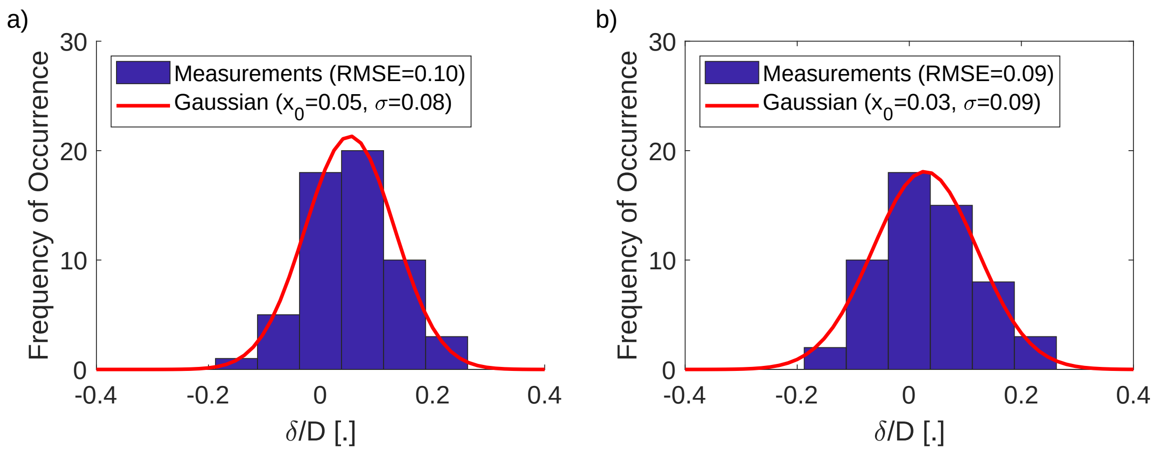

Figure 8. Histograms of the normalized wake deflection δ/D at $x/D = 4$ for the control cases with a successful wake-center detection. The left panel (a) shows the normalized wake deflection based on the yaw angle from the WindIris (γ_{WI}) and the right panel (b) for the yaw angle of the WindCube (γ_{WC}). Both 2D and 3D scans of wake-scanning lidar for control cases with a successfully detected wake center are used.

model overestimates it. These qualitative observations from this example case will be extended to all wake-steering cases in the following.

The wake deflection at a downwind distance of $x/D = 4$ is shown in Fig. ~~??e~~9b for all wake-steering cases with a sucessfull wake-center detection. The observed wake deflection increases with the yaw angle as expected from wind tunnel experiments (Bastankhah and Porté-Agel, 2016) and numerical simulations (Lin and Porté-Agel, 2019). The analytical model of Jiménez et al. (2009) overestimates the wake deflection, and the models by Bastankhah and Porté-Agel (2016) and Qian and Ishihara (2018) better match the wake deflection from the field measurements. The overestimation of the Jiménez et al. (2009) model was also observed by Bastankhah and Porté-Agel (2016) with wind tunnel experiments and by Lin and Porté-Agel (2019) with numerical simulations. The measurement data shows considerably larger scattering than the model predictions, which is likely a consequence of the remaining ~~non-stationarity~~ nonstationarity of the atmospheric boundary layer in the dataset and the measurement errors of the ~~measurement data~~yaw angle. It should be noted that the short downwind distance of $x/D = 4$ at which the models are evaluated is heavily influenced by the wake skew angle assumed for the near wake, which is used to provide an initial condition for the ~~far-wake~~far wake. The similar wake deflections for the Bastankhah and Porté-Agel (2016) model and the Qian and Ishihara (2018) model are then explained by the identical wake skew angle used by both models (Eq. 10 and Eq. 22), and noticeable differences of the wake deflection between these two models only appear at larger x/D~~(Lin and Porté-Agel, 2019). Further, for cases with very low turbulence intensities, the models were not able to make a prediction at $x/D = 4$, because the predicted length of the near wake was longer. However, since the turbine spacing within a wind farm can be relatively short (here $5D$), this highlights the importance of a near wake description in the analytical models.~~
.

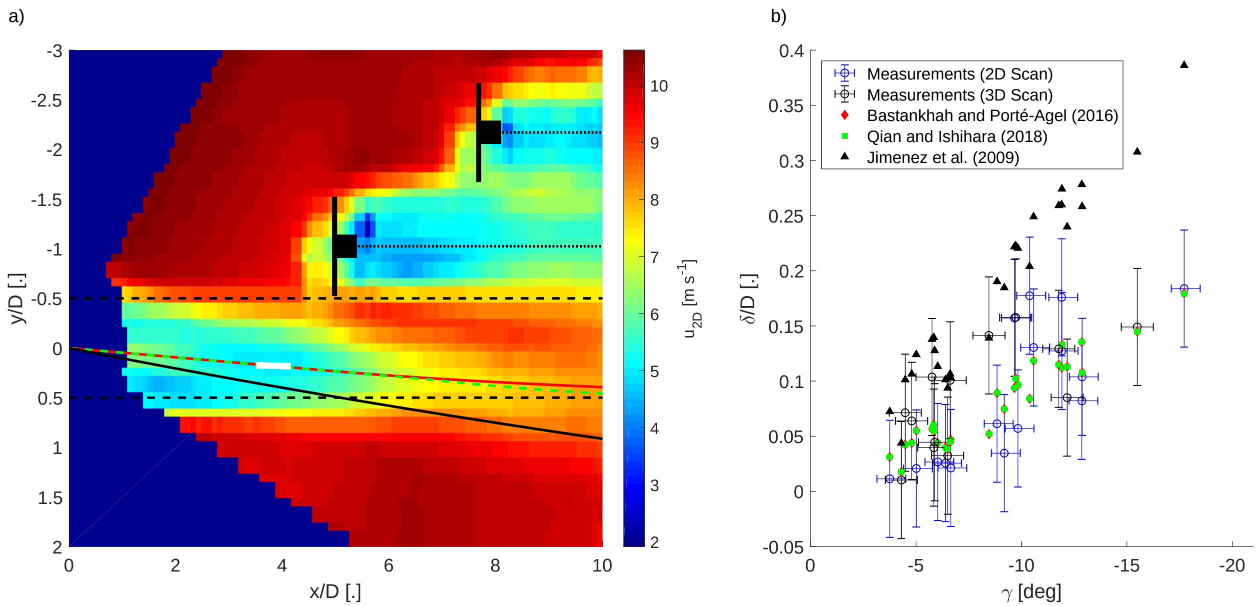

Figure 9. ~~Example case of~~ The left panel (a~~yawed wind turbine wake~~) shows an example from the wake-steering cases with a mean yaw ~~angle~~ offset of $\gamma = 18°$. The mean longitudinal velocity field is shown as a colour image. The predicted wake deflection of the Bastankhah and Porté-Agel (2016) model is shown as a red solid line, the Qian and Ishihara (2018) model is shown as a green dashed line, and the Jiménez et al. (2009) model is shown as a black solid line. The ~~dashed~~ solid white line shows the result of the wake center detection ~~and the solid white line indicates the part~~ with a correlation coefficient larger than 0.99 (see Sect. 2.3.3). The black dashed line indicates the rotor area of T2. ~~Turbine~~ Turbines 3 and 4 are stylized in black, and a black dotted line as ~~an~~ a visual aid to indicate the downwind direction. The right panel (b) shows the normalized wake deflection at $x/D = 4$ as a function of the yaw angle for the wake-steering cases with a successful wake detection and a model prediction at $x/D = 4$. The measurements are shown in blue for the 2D scans and in black for the 3D scans. The errorbars are based on the errors found between WindIris and WindCube (Sect. 3.1). The analytical models of Jiménez et al. (2009) (black triangles, Eq. A25), Bastankhah and Porté-Agel (2016) (red diamonds, Eq. A7), and Qian and Ishihara (2018) (green squares, Eq. A18) are plotted for each case.

~~The two top panels show a histogram of the normalized wake deflection δ/D at $x/D = 4$ for the control cases based on the yaw angle γ from the WindIris (a) and the WindCube wind direction and the nacelle position of T2 (b). The bottom panel (c) shows the normalized wake deflection at $x/D = 4$ as a function of the yaw angle for the wake steering cases. Here, the yaw angle from WindIris and WindCube were averaged. The measurements are shown in blue for the 2D scans and in black for the 3D scans. The errorbars are based on the errors found between WindIris and WindCube (Sect. 3.1). The analytical models of Jiménez et al. (2009) (black triangles, Eq. A25), Bastankhah and Porté-Agel (2016) (red diamonds, Eq. A7), and Qian and Ishihara (2018) (green squares, Eq. A18) are plotted for each case.~~

3.3 Power

The ~~power estimated from the velocity field~~ velocity fields predicted by the analytical models ~~is investigated~~and measured by the Doppler lidars are used to estimate the power of the wind turbines. First, the power estimated from the Doppler lidars is compared with the SCADA data. Afterwards, the predictions of the three analytical models are validated against the SCADA data and the measurements of the ~~wake scanning lidar. Then, the effect of wake steering on the power of the downwind turbine (T3) and the full system of upwind and downwind turbine (T2+T3) is investigated.~~ wake-scanning lidar. The investigation is carried out for ~~periods classified as wake steering~~ the wake-steering cases with a 3D scan of the ~~wake scanning lidar~~ wake-scanning lidar and a model prediction at $x/D = 4$ (Table 1).

3.3.1 ~~Model validation for~~ Estimated power from the Doppler lidars

The power estimated from the measurements of the Doppler lidars (Eq. 6 and Eq. 7) is compared with the SCADA data~~(Fig. ??).~~. The power of T2 ~~computed~~ from the WindCube ~~measurements~~ and the SCADA ~~have correlation coefficient of 0.98 and a RMSE of 69 kW~~ data (Fig. ~~??a) . The power differences between the WindCube and the SCADA data show no relationship to the yaw angle indicating that the adjustment of the power coefficient of a yawed turbine with $\cos^3\gamma$ as proposed by Adaramola and Krogstad (2011) holds for the field data. The power of~~ 10a) has better agreement than the power of T3 ~~has a correlation coefficient of 0.97 and a RMSE of 132 kW between the wake scanning~~ from the wake-scanning lidar and the SCADA data (Fig. ~~??~~10b). A ~~bias is not apparent for T2 nor for T3. One possible reasons~~ possible reason for the larger errors for T3 could be that the ~~power coefficient curve used to compute the power is not ideal for cases with an inhomogeneous wind field across the rotor, if~~ specification of the power coefficient is problematic for a waked wind turbine, because T3 is ~~partially waked as it is frequently the case in the data set. A second reason could be the influence of the induction zone in combination with a power curve that is based on the free stream velocity~~usually waked by T2 for the wake-steering cases. The differences between the wake-scanning lidar and the WindCube are less likely an explanation, because the wake-scanning lidar has a higher measurement density across the rotor area and a more favorable scan geometry. The power differences between the WindCube and the SCADA data show no relationship to the yaw angle (not shown), indicating that the adjustment of the power coefficient of a yawed turbine with $\cos^3\gamma$ holds for the field data.

~~A~~

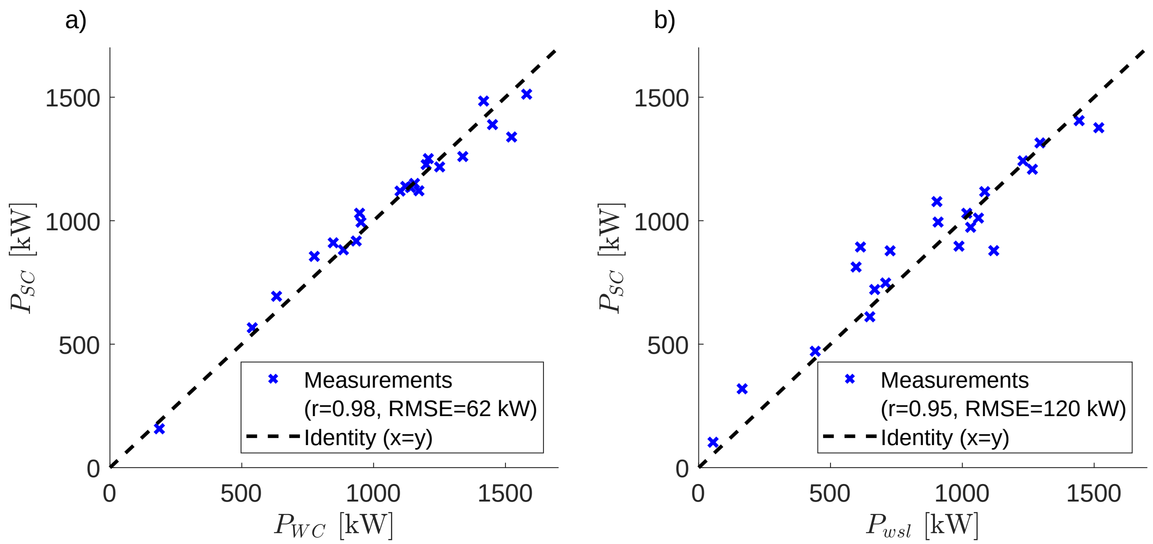

Figure 10. Comparison of the power from the SCADA data and the power estimated from the Doppler lidar measurements for T2 (a) and T3 (b) using the wake steering cases with a 3D scan of wake-scanning lidar and a model prediction at $x/D = 4$. Blue crosses show the measurement data, and the black dashed line is the identity ($y = x$).

3.3.2 Model validation for the power

The model validation will be carried out in three steps to distinguish various error contributions. Starting with a comparison of the ~~power computed~~ rotor-averaged velocity of T3 from the Bastankhah and Porté-Agel (2016) model, the Qian and Ishihara (2018) model, and the Jiménez et al. (2009) model with the measurements ~~is shown in Fig ??~~of the wake-scanning lidar (Fig 11a). The Qian and Ishihara (2018) model ~~has a RMSE of 98 kW with the wake scanning lidar and 172 kW with the SCADA data with correlation coefficients of 0.98~~ and ~~0.93 respectively. The Bastankhah and Porté-Agel (2016) model has a RMSE of 103 kW with the wake scanning lidar and 193 kW with the SCADA data with the same correlation coefficients as the Qian and Ishihara (2018) model. The Jiménez et al. (2009) model has an RMSE of 211 kW with the wake scanning lidar, 224 kW with the SCADA data and correlation coefficients of 0.96 and 0.92, respectively~~the Bastankhah and Porté-Agel (2016) model have both an error of 5%. The Jiménez et al. (2009) model has considerably larger ~~errors~~ error than the other two models ~~,~~because it assumes a top-hat velocity deficit that overestimated the velocity deficit at the edges of the wake, which resulted in an underestimation of the ~~power~~ rotor-averaged velocity for a partially waked downwind turbine. The Gaussian velocity deficits of the other two models better matched the Doppler lidar observations in this respect. The ~~better agreement with the wake scanning lidar than with the SCADA data supports the assumption that the power coefficient has problems with partially waked turbines.Several factors contribute to the error of the analytical models: the physical simplifications,~~ model input values are subject to measurement errors, which propagated into an uncertainty of the model error. This uncertainty is estimated by varying the model input values based on the errors found in Sect. 3.1. The error propagation of γ and TI_{WI} introduces an uncertainty of less than 0.5%, while the error propagation of u_{WC} and dir_{WC} had an effect of 2% and 1%, respectively.

A comparison of the power of T3 from the analytical models with the wake-scanning lidar is shown in Fig 11b. The increased error percentages compared to the rotor-averaged velocity in Fig 11a are explained by the error magnification due to the cubed velocity in the computation of the power.

A further increase of the ~~errors of the input parameters, and the errors from the inflow scanning WindCube that propagate into the longitudinal velocity field. Assuming the~~ error ~~between the power estimated from the WindCube and the SCADA data of T2 as a proxy for the propagated error , the Qian and Ishihara (2018) model and the Bastankhah and Porté-Agel (2016) model would have a RMSE~~ is observed if the analytical models are combined with the power curve of the wind turbine for comparison with the SCADA ~~that is comparable to the wake scanning lidar~~data (Fig 11c). This is in line with the assumption from the previous section that the specification of the power coefficient is problematic for waked wind turbines. Using different methods to estimate the power coefficient does not affect the overall findings (e.g., using the velocity in front of the nacelle instead of averaging the rotor area or switching between the model prediction and the lidar measurement). The average error propagation from the WindCube measurements is estimated to be 52 kW, which roughly agrees with the error between the power estimated from the WindCube and the SCADA data of T2 (Fig. 10a) and highlights the fact that the found errors are not only due to the models, but include significant contributions from the measurement errors.

3.3.3 ~~Effect of wake steering on the power: example case~~

3.4 Effect of wake steering on the power

The effect of wake steering on the power of the downwind turbine (T3) and the full system of upwind and downwind turbine (T2+T3) is first investigated with a case study and afterwards using the wake-steering cases with a 3D scan of the wake-scanning lidar and a model prediction at $x/D = 4$ (Table 1).

3.4.1 Case study of the wake steering

The ~~dataset~~ data set is searched for pairs of 30-minute periods with T3 downwind of T2 and similar inflow conditions, but one being yawed and the other not. All periods where the wind direction was aligned with the downwind turbine within 1° were ordered by the wind speed, and two suitable pairs were identified (Fig. ~~??a and ??~~12a and Fig. 12b). In the case of the second pair, the turbulence intensity was too low for the analytical model to make a prediction at $x/D = 4$ and~~therefore~~, therefore, only the first pair is discussed in the following.

The inflow measurements and the power output of the turbines of the example case are summarized in Table ~~??a~~2a, and the longitudinal mean velocity fields of the ~~wake scanning~~ wake-scanning lidar are shown in Fig. ~~??d and ??~~12d and Fig. 12e. The increase of wind speed ~~and the decrease of wind shear from the yawed to the non-yawed case~~ together with the power losses of the yawed turbine, could explain the power ~~difference~~ increase for T2 from the yawed to the nonyawed case seen in

~~Comparison of the power from the SCADA data and the power estimated from the Doppler lidar measurements for T2 (a) and T3 (b). Blue crosses show the measurement data and the black dashed line is the identity ($y = x$).~~

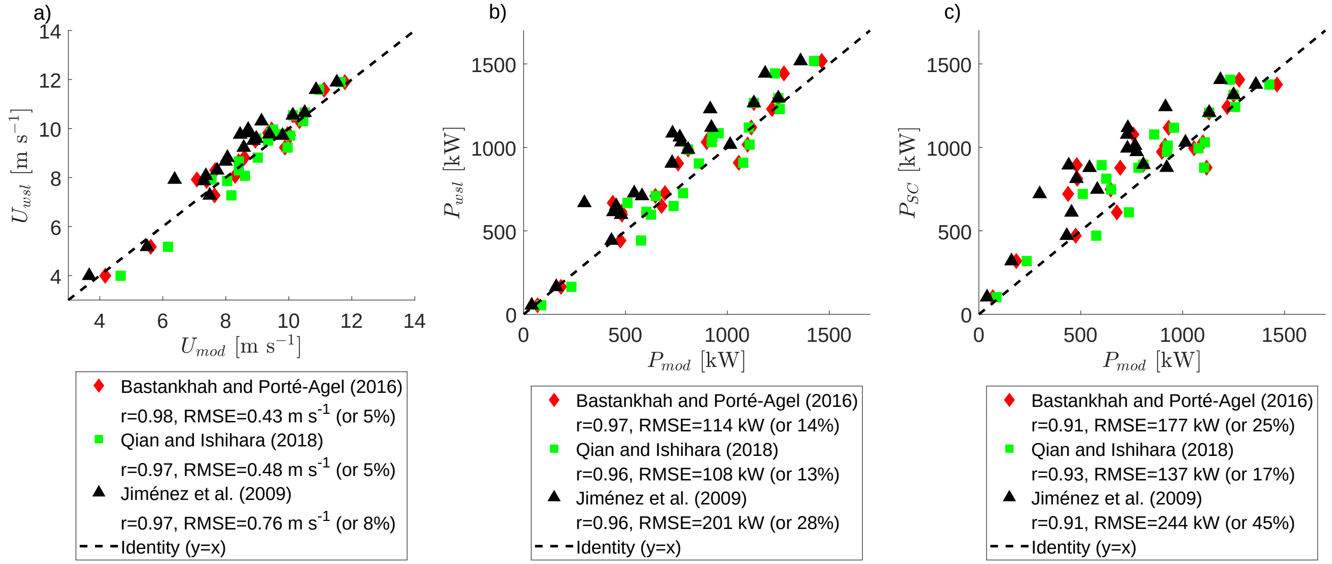

Figure 11. The ~~power~~ for rotor-averaged velocity prediction of the analytical models for T3 compared with the ~~wake scanning~~ measurements by wake-scanning lidar (a). The power prediction of the analytical models for T3 compared with the wake-scanning lidar (b) and the SCADA data (~~b~~c). Data of the wake-steering cases with a 3D scan of wake-scanning lidar and a model prediction at $x/D = 4$ is used. Red diamonds show the Bastankhah and Porté-Agel (2016) model, green squares show the Qian and Ishihara (2018) model, black triangles show the Jiménez et al. (2009) model, and the black dashed line is the identity.

the SCADA data. For T3, the SCADA data reports higher power for the case with wake steering compared to the case without wake steering, which could be explained by the deflection of the wake.

Using the Qian and Ishihara (2018) model and the inflow measurements to predict the power of the turbines captures the tendencies ~~,~~ but underestimates the power for T3 (Table ~~??~~2b). The effect of the wake steering can be isolated by averaging TI_{WI} and $u_{WC}(z)$ for both cases and only varying γ (Table ~~??~~2c). Conversely, the effect of the inflow conditions can be isolated by setting $\gamma = 0°$ and using TI_{WI} and $u_{WC}(z)$ as measured (Table ~~??~~2d). The results ~~confirm~~ show that the wake steering had an effect on the power of T3, and changes of the inflow alone cannot explain the power differences between the yawed and the ~~non-yawed~~ nonyawed case. Based on the analytical model and the SCADA data, the yawed T2 lost 60–80 kW and the T3 gained 90–170 kW by the wake steering. ~~The Bastankhah and Porté-Agel (2016) model had qualitatively similar results, but approximately 20 to 30 kW smaller than the Qian and Ishihara (2018) model.~~ As a side note, it was observed that wake steering is not necessary at high wind speeds ~~,~~ because the wake has enough available power for the downwind turbine to run at its rated capacity (Fig. ~~??~~12c).

Using yawed and ~~non-yawed~~ nonyawed cases with similar inflow conditions as above to investigate the effect of wake steering for a wider part of the data set is not feasible due to the limited number of suitable pairs. However, this example case

Table 2. Inflow and power output for the yawed case (left column) and ~~non-yawed~~ nonyawed case (right column) shown in Fig. ~~??~~12d and Fig. ~~??~~12e. The upper part (a) presents the inflow measurement from the Doppler lidars and power from the SCADA data. The lower three parts show the power estimated from the inflow profiling lidar for T2 and the prediction of the Qian and Ishihara (2018) model for T3 based on the inflow values (b), the averaged inflow values only varying γ (c), and the inflow values with $\gamma = 0$ (d).

	Description		Yawed	Non-yawed
a)	Inflow and SCADA	γ [deg]	-12.5	-0.2
		$dir_{WC}(z_{hub})$ [m s^{-1}]	323.3	232.2
		$u_{WC}(z_{hub})$ [deg]	10.3	10.5
		TI_{WI} [.]	0.05	0.07
		$P_{T2,SC}$ [kW]	1134	1197
		$P_{T3,SC}$ [kW]	894	790
b)	Inflow and wake steer.	$P_{T2,WC}$ [kW]	1105	1183
		$P_{T3,mod}$ [kW]	822	668
c)	Averaged inflow	$P_{T2,WC,avg}$ [kW]	1093	1175
		$P_{T3,mod,avg}$ [kW]	827	655
d)	No wake steering	$P_{T2,WC,\gamma=0}$ [kW]	1187	1183
		$P_{T3,mod,\gamma=0}$ [kW]	733	667

illustrated that using an analytical model to artificially remove the wake steering captures the power changes and can be used to investigate the effect of wake steering on the power.

3.4.2 ~~Effect of wake~~ Wake steering ~~on the power: complete data set~~evaluation

The effect of wake steering on the power is investigated using the periods classified as ~~wake steering~~ wake-steering cases. The data for 12 and 24 January 2019 have been excluded from this part of the analysis ~~,~~ because the yaw controller had toggling issues. The data set will be divided into two groups based on the wind direction following a visual inspection of the volumetric lidar measurements, which showed two categories of ~~wake steering~~ wake-steering cases:

1. Successful wake steering, where the wake of the yawed T2 was partially or completely deflected away from T3 (Fig. ~~??a and ??~~13a and Fig. 13b).

2. Unnecessary or harmful wake steering, where the wake of the yawed T2 would have missed T3 even if T2 would not have yawed (Fig. ~~??c and ??~~13c and Fig. 13d) or where the wake of the yawed T2 was deflected on T3 instead of away (Fig. ~~??e and ??~~13e and Fig. 13f).

~~The latter group is expected to be detrimental to the overall power output, because the unnecessary wake steering decreases the power output of the upwind turbine without gains for the downwind turbine and the harmful wake steering case decreases the power output of both turbines.~~ Geometrical considerations of the rotor area shadow of T2 in the wind direction can explain

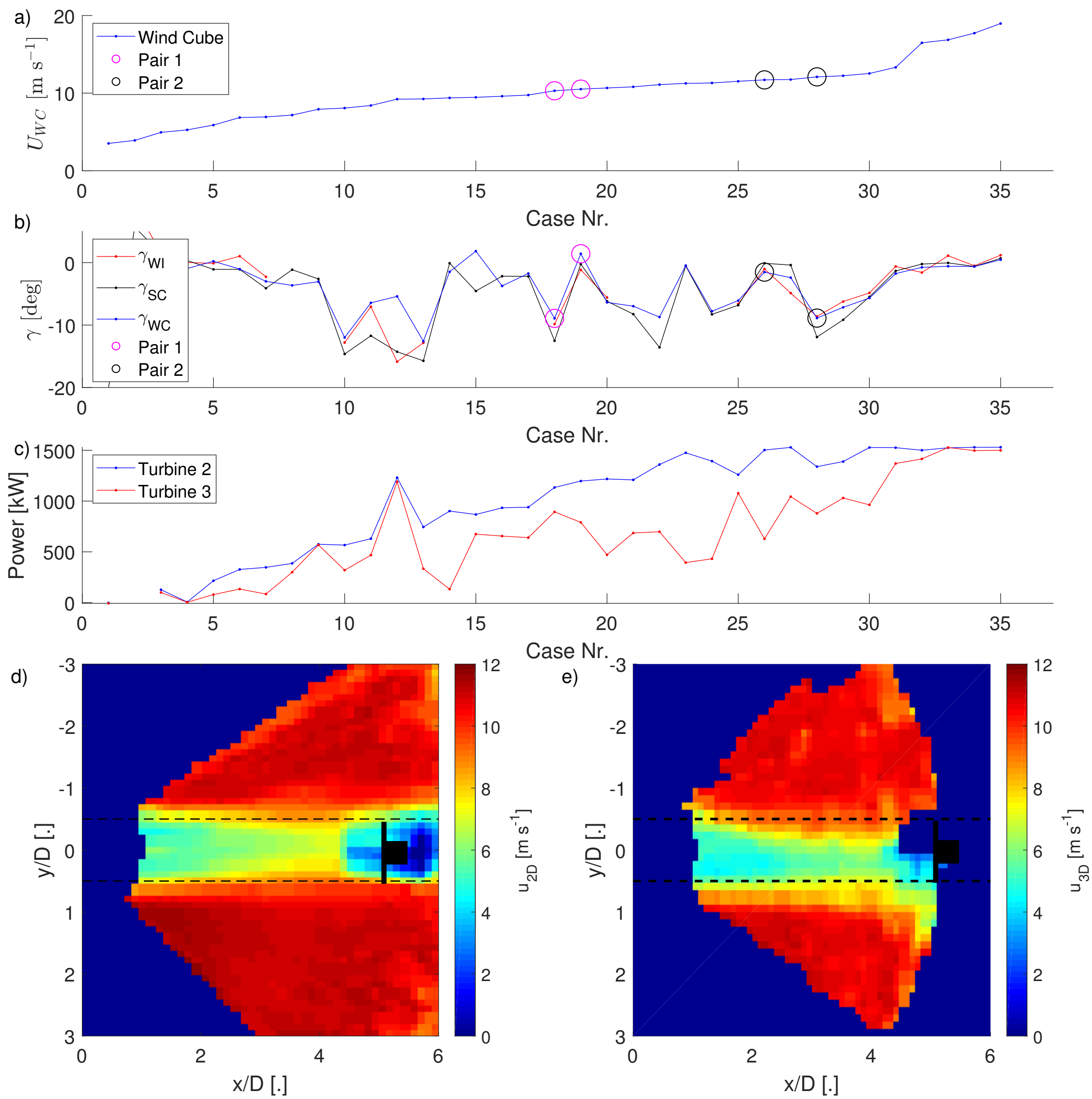

Figure 12. The inflow wind speed (a), the yaw angle of T2 (b), and the power (c) for all 30-minute periods with the wind direction aligned with the downwind turbine within 1° sorted by wind speed (data filtering of Sect. 2.3.1 not applied). Highlighted with circles are the two pairs with similar wind speed and wind direction and all measurement data available, but different yaw angles. The two bottom panels show the mean longitudinal velocity fields at hub height from the ~~wake scanning~~ wake-scanning Doppler lidar for the first pair with the ~~non-yawed~~ nonyawed case on the left (d) and the yawed case on the right (e). The rotor area shadow of T2 is indicated as a black dashed line, and the position of T3 is stylized in black.

the unnecessary cases. The harmful ~~wake steering~~ wake-steering cases were observed for wind directions very close or smaller than the direction ~~towards~~ toward T3 and might be explained by ~~errors~~ the bias of the wind direction perceived by the wind turbine under yawed conditions (Fig. ~~??~~7b) or the variability of the wind direction during the scan period (Simley et al., 2019). Therefore, the ~~wake steering cases are separated into two groups: a~~ effect of wake steering will be investigated separately for a subgroup with a narrow inflow sector from 325° to 335° ~~and a wide inflow sector from 310° to 350°.~~ in addition to all wake-steering cases.

The effect of wake steering on the power of the downstream turbine (T3) is investigated based on the ~~differences between the power predicted by the Qian and Ishihara (2018) model for the inflow parameters and a hypothetically non-yawed case with the same inflow conditions otherwise.The results for the downwind turbine are shown~~ wake-scanning lidar (Sect. 2.3.4), and based the Qian and Ishihara (2018) model (Sect. 2.4). The results in Fig. ~~?? and summarized in Table ??. An average power improvement of 72 kW (or 9%)~~ 14 show an power increase for T3 for the ~~narrow group that is reduced to 22 kW (or 2%) for the wide group indicates that several periods in the wide group had~~ cases with a wind direction between 325° and 335°, but the cases outside of this wind direction range have very small power gains ~~or~~ of even power losses~~for T3.~~. Table 3 summarizes these findings and also includes the power gains of the combined system of upstream and downstream turbine. The combined system that includes the power losses of the yawed upstream turbine (T2) has a power improvement ~~23 kW (or 2%)~~ of 2-3% for the narrow ~~group and~~ wind direction sector, but shows virtually no improvement for the ~~wide group (2 kW or 0%). The Bastankhah and Porté-Agel (2016) model provided qualitatively similar results to the Qian and Ishihara (2018) model (T3 power gains of 11% for the narrow group that are reduced to 3% for the wide group). For both models, the~~ wider wind direction sector. The harmful or unnecessary ~~wake steering~~ wake-steering cases were reducing the power gains significantly for the ~~wake steering set-up~~ wake-steering setup in this study. These findings are in line with ~~Simley et al. (2020)~~the findings of Simley et al. (2020) using a SCADA data driven approach.

3.5 ~~Shape of the wake~~

4 Summary and Conclusions

Field measurements of yawed wind turbine wakes ~~with~~ were performed with a nacelle-mounted scanning Doppler ~~lidars were performed~~lidar. The wake was ~~characterized~~ characterised in terms of depth, width, and deflection from planar and volumetric scans of the Doppler ~~lidars~~lidar. Together with the inflow measurements, this data was used for validation of ~~the wake deflection and the power predictions of three analytical models for yawed wind turbine wakes.~~ three analytical wake models and evaluating the wake-steering setup.

The observed wake deflection increased with the yaw angle, and the comparison to the analytical models showed an overestimation by the Jiménez et al. (2009) model, while the Bastankhah and Porté-Agel (2016) model and the Qian and Ishihara (2018) model matched the measurement data better. The ~~predicted power~~ predictions of the Qian and Ishihara (2018) model ~~had the smallest errors with 17% compared to the SCADA data and 12% compared to the power estimated from the Doppler lidar measurements. Followed by the Bastankhah and Porté-Agel (2016) model with errors of 24%~~and ~~13%, respectively, and~~

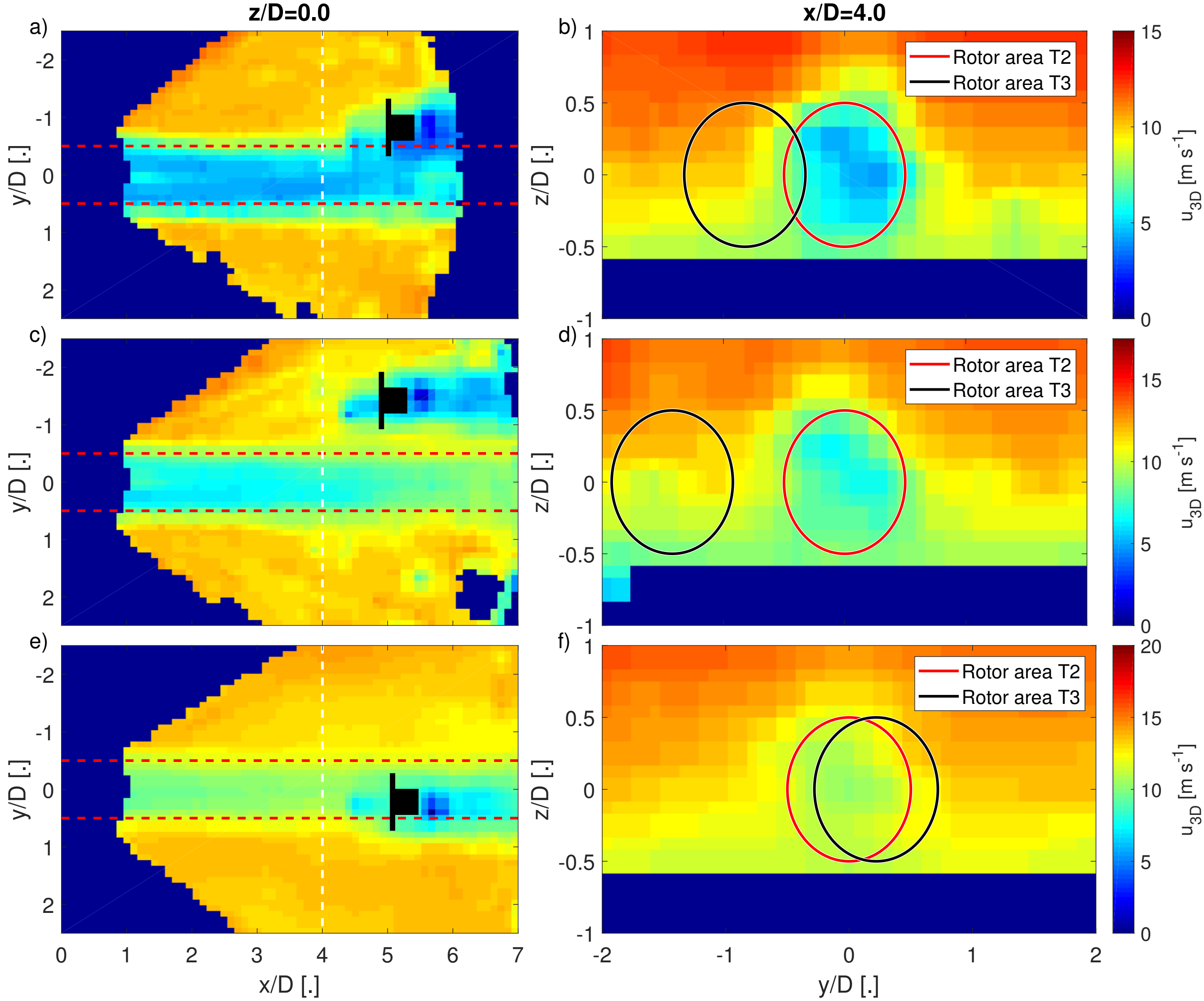

Figure 13. ~~Examples for observed categories~~ Three examples selected from the wake-steering cases to illustrate successful and detrimental cases of ~~wake steering~~wake-steering. The top row (a,b) shows a successful ~~wake steering~~ wake-steering case. The middle row (c,d), shows an unnecessary wake steering case. The bottom row (e,f) shows a harmful ~~wake steering~~ wake-steering case. The colour scale shows the longitudinal velocity of the ~~wake scanning~~ wake-scanning Doppler lidar. The left column shows a horizontal ~~cross-section~~ cross section of the longitudinal velocity at hub height. The right column shows ~~a~~ spanwise ~~cross-sections~~ cross sections of the longitudinal velocity at a downwind distance of $4D$. The red dashed lines and red solid circles show the outline of the rotor area of T2 in wind direction. The position of T3 is stylized in black, and the black solid circle shows the rotor area of T3.

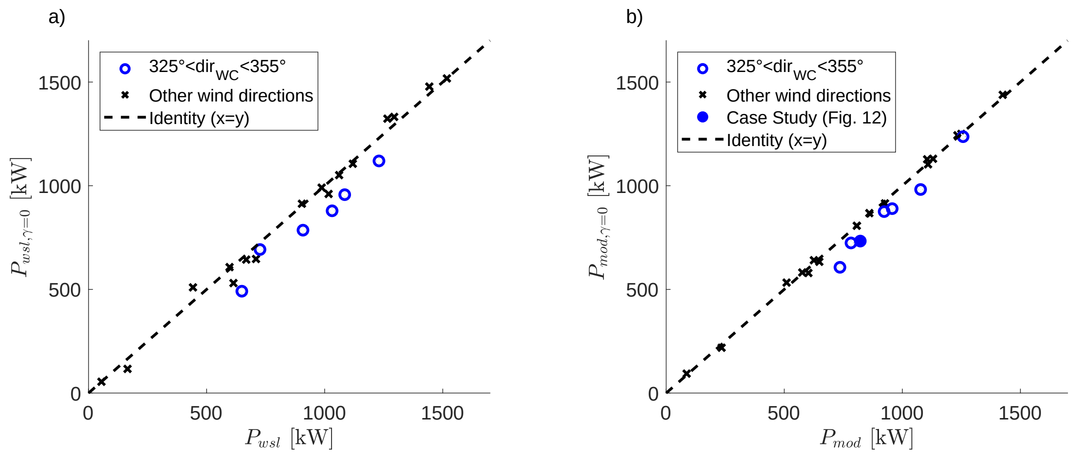

Figure 14. The effect of wake steering on the power ~~based on~~ of the ~~Qian and Ishihara (2018) model. The left panel~~ downstream turbine (~~a~~T3) ~~shows the effect~~ based on the ~~power for the downwind turbine~~ wake-scanning lidar (~~T3~~a), and the ~~right panel~~ Qian and Ishihara (2018) model (b)~~for~~. Data of the ~~combined system~~ wake-steering cases with a 3D scan of ~~upwind~~ wake-scanning lidar and ~~downwind turbine (T2+T3)~~a model prediction at $x/D = 4$ is used. The hollow blue circles indicate data points from the narrow inflow sector, the black crosses are data points ~~from~~ outside of the ~~wide~~ narrow inflow sector, and the solid blue circle is the yawed example case from ~~Sect~~Fig. ~~??~~12.

Table 3. Maximum and average power gains and losses due to wake steering for the ~~narrow~~ subgroup with wind directions between 325° and 335° and considering all wind directions. The two left columns show the ~~wide group~~ power changes based on the wake-scanning lidar, the two right columns show the power changes based on the Qian and Ishihara (2018) model. The ~~two left columns show~~ results of the downwind turbine (T3) and the ~~two right columns show the~~ combined system of upwind and downwind turbine (T2+T3) are shown for both. The percentage values are based on the power of the yawed case. Data of the wake-steering cases with a 3D scan of wake-scanning lidar and a model prediction at $x/D = 4$ is used.

	wake-scanning Doppler lidar				Qian and Ishihara (2018) model			
	T3		T2 + T3		T3		T2 + T3	
	325° to 335°	All	325° to 335°	All	325° to 335°	All	325° to 335°	All
Max. gain	24%	24%	4%	4%	18%	18%	3%	3%
Avg. gain	13%	11%	3%	3%	8%	4%	2%	1%
Avg. loss	NA	-4%	0%	-2%	NA	-3%	0%	-1%
Max. loss	NA	-12%	0%	-5%	NA	-5%	-1%	-3%
Overall	13%	5%	3%	1%	8%	3%	2%	0%

the Bastankhah and Porté-Agel (2016) model for the rotor-averaged velocity of the downstream turbine had errors of 5%, while the Jiménez et al. (2009) model ~~that had the largest errorswith 40% and 28%. For comparison, the power estimated from the Doppler lidar measurements~~ had considerably larger errors. These model errors include the error propagation from the inflow measurements that are used as input for the analytical models. Power predictions using the analytical models had an error ~~of 14% to the SCADA data. The~~ magnification due to the cubed velocity in the computation of the power. Further, the specification of the power coefficient for ~~an inhomogeneous wind field across the rotor area, if the downwind turbine is partially waked , was identified as an error source among others. Further, it was found that some cases of wake steering were~~ the calculation of the power output from the waked wind turbine was shown to be a problematic issue.

The wake-steering in this setup was not working optimally, with some cases even being detrimental to the power output. The wake-scanning lidar and the Qian and Ishihara (2018) model both showed that the wake was not always deflected away from the downwind turbine. The combination of the bias of the wind vane on top of the nacelle when the turbine was yawed, the variability of the wind direction within the averaging period, and the implemented ~~wake steering~~ wake-steering design could explain those cases~~and highlights the importance to develop a wake steering set-up that is robust against those problems . Lastly, it was observed that the wind veer had a dominant effect on the spanwise shape of the wake and kidney-shaped wakes were not observed in the field data. Application of the analytical model~~. Narrowing the wind direction range for which a yaw offset is applied mitigated those problems to some extend, but is not an optimal solution. Especially the bias of the wind vane when the turbine is yawed should receive further attention, because it could result from a flow distortion in the proximity of the nacelle during yawed operation, which would point to a problem of the standard wind turbine instrumentation to provide the input measurements for the wake steering with the needed quality. It might be possible to correct this bias in the yaw controller with a turbine specific correction function, if it only depends on the yaw angle and the wind speed. A forward facing Doppler lidar could solve this problem and it could also open up the possibility for measurements of the incoming turbulence level. Using an external wind direction measurement like the Wind Cube in this study is problematic for large wind farms due to the horizontal homogeneity assumption.

Application of analytical models to predict the power of waked downstream turbines would benefit from a power coefficient adapted to an inhomogeneous wind field across the rotor area ~~,~~ and an improved description of the near wake for better handling of short turbine spacing or low turbulence intensities~~, and accounting for non-stationary and inhomogeneous boundary layers.~~ . A kidney shape of the wake cross section was not observed, which is likely explained by the dominant effect of the wind veer on the spanwise shape of the wake (Appendix B). Non-stationarity of the boundary layer, which cannot be handled by the analytical model, was the most limiting factor in the selection of suitable periods for the validation.

Data availability. The data is not publicly available due to a non-disclosure agreement with the wind farm operator.

Appendix A: Equations of the analytical models

The equations of the three analytical models compared in this article are summarized from their respective publication for convenience.

A1 Bastankhah and Porté-Agel (2016)

The analytical model from Bastankhah and Porté-Agel (2016) is based on the conservation of momentum and assumes a Gaussian distribution of the velocity deficit. The wake skew angle in the near wake is given by:

$$\theta_0 = \frac{0.3\gamma}{\cos(\gamma)}(1-\sqrt{(1-C_T\cos(\gamma))} \tag{A1}$$

with γ given in radiant. The length of the near wake is given by:

$$x_0 = \frac{\cos(\gamma)(1+\sqrt{1-C_T})}{\sqrt{2}(\alpha TI_x+\beta(1-\sqrt{1-C_T}))}D \tag{A2}$$

with $\alpha = 2.32$ and $\beta = 0.154$. The width of the wake in the far wake ($x \geq x_0$) is given by:

$$\sigma_y(x) = k_y^*(x-x_0)+\frac{\cos(\gamma)}{\sqrt{8}}D \tag{A3}$$

for the vertical direction and by:

$$\sigma_z(x) = k_z^*(x-x_0)+\frac{1}{\sqrt{8}}D \tag{A4}$$

for the transversal direction. The wake growth rate is assumed to be isotropic in the spanwise plane and proportional to the turbulence intensity with

$$k_y^* = k_z^* = 0.35TI_x \tag{A5}$$

following results of a field campaign (Fuertes et al., 2018). For $TI_x < 0.06$, the wake growth rates are set to 0.021 to account for the turbulence induced by the turbine itself. The wake deflection from the line of wind direction at the onset of the far wake is given by:

$$\delta_0 = \tan(\theta_0)x_0 \tag{A6}$$

and for the far wake ($x \geq x_0$) by:

$$\delta(x) = \delta_0 + \frac{D\tan(\theta_0)}{14.7}\sqrt{\frac{\cos(\gamma)}{k_y^*k_z^*C_T}}(2.9+1.3\sqrt{1-C_T}-C_T)\log\left(\frac{a}{b}\right) \tag{A7}$$

with

$$a = (1.6+\sqrt{C_T})(1.6\sqrt{\frac{8\sigma_y\sigma_z}{D^2\cos(\gamma)}}-\sqrt{C_T}) \tag{A8}$$

and

$$b = (1.6 - \sqrt{C_T})(1.6\sqrt{\frac{8\sigma_y\sigma_z}{D^2\cos(\gamma)}} + \sqrt{C_T}). \tag{A9}$$

Lastly, the velocity deficit is computed with

$$\frac{\Delta u}{u_{hub}} = \left(1 - \sqrt{1 - \frac{C_T\cos(\gamma)}{8\sigma_y\sigma_z/D^2}}\right)\exp\left(-0.5\frac{(y-\delta)^2}{\sigma_y^2}\right)\exp\left(-0.5\frac{z^2}{\sigma_z^2}\right). \tag{A10}$$

A2 Qian and Ishihara (2018)

The model of Qian and Ishihara (2018) also uses a Gaussian distribution of the velocity deficit. The different definition of the thrust coefficient used in Qian and Ishihara (2018) is related to definition employed here by $C'_T = C_T\cos(\gamma)$. The wake growth rate is given by:

$$k^* = 0.11 C_T'^{1.07} TI_x^{0.20} \tag{A11}$$

and the potential wake width at the rotor plane is given by:

$$\epsilon^* = 0.23 C_T'^{-0.25} TI_x^{0.17}. \tag{A12}$$

The wake skew angle in the near wake is given by:

$$\theta_{x0} = \frac{0.3\gamma}{\cos(\gamma)}(1 - \sqrt{1 - C'_T\cos^3(\gamma)}) \tag{A13}$$

and the wake width at the onset of the far wake is given by:

$$\sigma_{x0} = \sqrt{\frac{C'_T}{\cos(\gamma)}\left(\frac{\sin(\gamma) + 1.88\cos(\gamma)\theta_{x0}}{44.4\theta_{x0}}\right)}D \tag{A14}$$

with the near wake length given by:

$$x_0 = \frac{D}{k^*}\left(\frac{\sigma_{x0}}{D} - \epsilon^*\right). \tag{A15}$$

The wake growth in the far wake is given by:

$$\sigma(x) = k^* x + \epsilon^* D \tag{A16}$$

and the wake deflection at the onset of the far wake is given by:

$$\delta_{x0} = \theta_{x0} x_0. \tag{A17}$$

The deflection of the wake center from the line of wind direction is given by integration of the wake skew angle in downwind direction (Howland et al., 2016) with

$$\delta(x) = \delta_{x0} + \frac{D\sqrt{C'_T/\cos^2(\gamma)}\sin(\gamma)}{18.24k^*}\log\left(\frac{c_1}{c_2}\right) \tag{A18}$$

with

$$c_1 = \left(\frac{\sigma_{x0}}{D} + 0.24\sqrt{C_T \cos^3(\gamma)}\right)\left(\frac{\sigma(x)}{D} - 0.24\sqrt{C_T \cos^3(\gamma)}\right) \tag{A19}$$

and

$$c_2 = \left(\frac{\sigma_{x0}}{D} - 0.24\sqrt{C_T \cos^3(\gamma)}\right)\left(\frac{\sigma(x)}{D} + 0.24\sqrt{C_T \cos^3(\gamma)}\right). \tag{A20}$$

The normalized velocity deficit is given by:

$$\frac{\Delta u}{u_{hub}} = F(C_T', TI_x, x/D)\exp\left(-\frac{x^2 + (y+\delta(x))^2}{2\sigma^2}\right) \tag{A21}$$

with

$$F(C_T', TI_x, x/D) = (a + bx/D + p)^{-2} \tag{A22}$$

and

$$a = 0.93 C_T'^{-0.75} TI_x^{0.17}, b = 0.42 C_T'^{0.6} TI_x^{0.2}, p = \frac{0.15 C_T'^{-0.25} TI_x^{-0.7}}{(1+x/D)^2}. \tag{A23}$$

A3 Jimenez et al. (2009)

The analytical model of Jiménez et al. (2009) is also based on the conversation of momentum, but assumes a top-hat distribution of the longitudinal velocity deficit. The wake growth rate is given by Eq. (A11) and the wake skew angle is given by:

$$\theta(x) = \frac{C_T \cos(\gamma)^2 \sin(\gamma)}{2(1+2k_w x/D)}. \tag{A24}$$

Integration of the wake skew angle in downwind direction provides the wake deflection, which is given by:

$$\delta(x) = \frac{\cos(\gamma)^2 \sin(\gamma) C_T}{4k_w}\left(1 - \frac{1}{1+2k_w x/D}\right)D. \tag{A25}$$

The normalized velocity deficit is given by:

$$\frac{\Delta u}{u_{hub}} = \frac{C_T D^2 \cos^3\theta}{2(D+k_w x)^2}, \tag{A26}$$

for $\sqrt{(y-\delta)^2 + z^2} \leq D + k_w x$ and zero outside. Other methods to compute the velocity deficit based on a top-hat distribution found in literature were tested, but resulted in larger errors (Peña et al., 2016; Frandsen et al., 2006).

Appendix B: Shape of the wake

The kidney-shaped spanwise cross sections of yawed-turbine wakes observed in wind tunnel experiments (Bastankhah and Porté-Agel, 2016 and numerical simulations (Howland et al., 2016; Lin and Porté-Agel, 2019) were not observed in the data from the field measurements.

Using the point vortex transportation model introduced by Zong and Porté-Agel (2020) it is shown that the effect of wind veer, which is frequently present in the atmospheric boundary layer, has a dominant effect on the shape of the wake. Even without wind veer, yaw angles smaller than 20° have a small effect on the shape of the wake that could be missed with the wake-scanning lidar. The strong effect of wind veer is in line with a simple assessment of the wake displacement based on the transversal advection due to the wind veer with:

$$\Delta y = x \tan\left(\frac{\alpha_{tt} - \alpha_{bt}}{D}(z - z_{hub})\right), \tag{B1}$$

where a wind veer of $\alpha_{tt} - \alpha_{bt} > 7°$ across the rotor area. It provides $\Delta y/D = 0.3$ for the bottom and top tips at $x/D = 5$ (Abkar et al., 2018). The effect of wind veer is not further analysed here because it has already been studied from field measurements in Bodini et al. (2017) and Brugger et al. (2019).

Author contributions. Conceptualization: F.P.-A.; Data curation: E.S., D.J., P.B., P.F., and M.D., Formal analysis: P.B.; Funding acquisition: F.P.-A., P.M.; Investigation: A.S., P.B., P.F., and M.M.; Methodology: P.B; Project administration: F.P.-A. and P.M.; Software: P.B, H.Z.; Supervision: F.P.-A., P.M.; Validation: P.B.; Visualization: P.B; Writing - original draft: P.B; Writing - review and editing: P.B., F.P.-A., M.D., A.S.,P.M., and D.J.;

Competing interests. The authors declare that they have no conflict of interest.

Acknowledgements. Fernando Porté-Agel, Haohua Zong, and Peter Brugger ~~recieved~~ received funding from the Swiss National Science Foundation [grant 200021-172538], the Swiss Federal Office of Energy, and the Swiss Innovation and Technology Committee (CTI) within the context of the Swiss Competence Center for Energy Research FURIES: Future Swiss Electrical Infrastructure. This work was authored in part by the National Renewable Energy Laboratory, operated by Alliance for Sustainable Energy, LLC, for the U.S. Department of Energy (DOE) under Contract No. DE-AC36-08GO28308. Funding provided by the U.S. Department of Energy Office of Energy Efficiency and Renewable Energy Wind Energy Technologies Office. The views expressed in the article do not necessarily represent the views of the DOE or the U.S. Government. The U.S. Government retains and the publisher, by accepting the article for publication, acknowledges that the U.S. Government retains a nonexclusive, paid-up, irrevocable, worldwide license to publish or reproduce the published form of this work, or allow others to do so, for U.S. Government purposes.

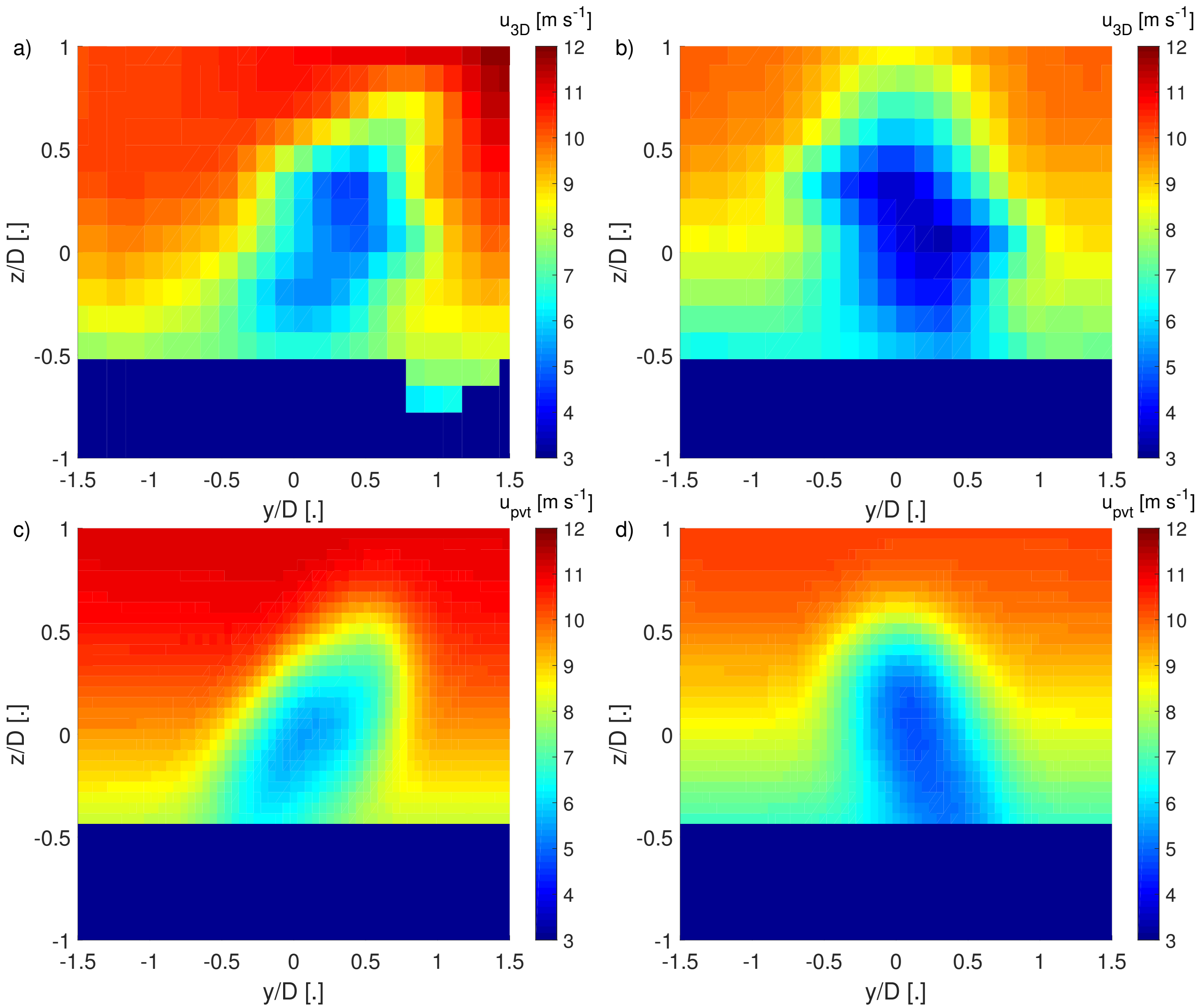

Figure B1. Spanwise cross sections of the longitudinal velocity field at $x/D = 4$. The top row (a,b) shows the velocity deficit from 3D scans of the wake-scanning Doppler lidar, and the bottom row (c,d) shows the results from the model of Zong and Porté-Agel (2020). The left column (a,c) is a case with a positive wind veer of $0.09°\ \mathrm{m}^{-1}$, and the right column (b,d) is a case with a negative wind veer of $-0.06°\ \mathrm{m}^{-1}$.

References

Abdulrahman, M. A.: Wind Farm Layout Optimization Considering Commercial Turbine Selection and Hub Height Variation, Ph.D. thesis, University of Calgary, https://doi.org/doi:10.11575/PRISM/28711, 2017.

Abkar, M., Sørensen, J. N., and Porté-Agel, F.: An Analytical Model for the Effect of Vertical Wind Veer on Wind Turbine Wakes, Energies, 11, https://doi.org/10.3390/en11071838, http://www.mdpi.com/1996-1073/11/7/1838, 2018.

Adaramola, M. and Krogstad, P.-.: Experimental investigation of wake effects on wind turbine performance, Renew. Energ., 36, 2078 – 2086, https://doi.org/https://doi.org/10.1016/j.renene.2011.01.024, http://www.sciencedirect.com/science/article/pii/S0960148111000462, 2011.

Annoni, J., Fleming, P., Scholbrock, A., Roadman, J., Dana, S., Adcock, C., Porte-Agel, F., Raach, S., Haizmann, F., and Schlipf, D.: Analysis of control-oriented wake modeling tools using lidar field results, Wind Energy Science, 3, 819–831, 2018.

Barthelmie, R. J., Pryor, S. C., Frandsen, S. T., Hansen, K. S., Schepers, J. G., Rados, K., Schlez, W., Neubert, A., Jensen, L. E., and Neckelmann, S.: Quantifying the Impact of Wind Turbine Wakes on Power Output at Offshore Wind Farms, J. Atmos. Ocean. Technol., 27, 1302–1317, https://doi.org/10.1175/2010JTECHA1398.1, https://doi.org/10.1175/2010JTECHA1398.1, 2010.

Bartl, J., Mühle, F., and Sætran, L.: Wind tunnel study on power output and yaw moments for two yaw-controlled model wind turbines, Wind Energy Science, 3, 489–502, https://doi.org/10.5194/wes-3-489-2018, https://wes.copernicus.org/articles/3/489/2018/, 2018.

Bastankhah, M. and Porté-Agel, F.: Experimental and theoretical study of wind turbine wakes in yawed conditions, J. Fluid Mech., 806, 506–541, https://doi.org/10.1017/jfm.2016.595, 2016.

Bastankhah, M. and Porté-Agel, F.: Wind tunnel study of the wind turbine interaction with a boundary-layer flow: Upwind region, turbine performance, and wake region, Physics of Fluids, 29, 065 105, https://doi.org/10.1063/1.4984078, https://doi.org/10.1063/1.4984078, 2017.

Bastankhah, M. and Porté-Agel, F.: A wind-tunnel investigation of wind-turbine wakes in yawed conditions, J. Phys. Conf. Ser., 625, 012 014, https://doi.org/10.1088/1742-6596/625/1/012014, 2015.

Bitar, E. and Seiler, P.: Coordinated control of a wind turbine array for power maximization, in: 2013 American Control Conference, pp. 2898–2904, https://doi.org/10.1109/ACC.2013.6580274, 2013.

Bodini, N., Zardi, D., and Lundquist, J. K.: Three-dimensional structure of wind turbine wakes as measured by scanning lidar, Atmos. Meas. Tech., 10, 2881–2896, https://doi.org/10.5194/amt-10-2881-2017, https://www.atmos-meas-tech.net/10/2881/2017/, 2017.

Bromm, M., Rott, A., Beck, H., Vollmer, L., Steinfeld, G., and Kühn, M.: Field investigation on the influence of yaw misalignment on the propagation of wind turbine wakes, Wind Energy, 21, 1011–1028, https://doi.org/10.1002/we.2210, https://onlinelibrary.wiley.com/doi/abs/10.1002/we.2210, 2018.

Brugger, P., Fuertes, F. C., Vahidzadeh, M., Markfort, C. D., and Porté-Agel, F.: Characterization of Wind Turbine Wakes with Nacelle-Mounted Doppler LiDARs and Model Validation in the Presence of Wind Veer, Remote Sens., 11, https://doi.org/10.3390/rs11192247, https://www.mdpi.com/2072-4292/11/19/2247, 2019.

Fleming, P., Annoni, J., Scholbrock, A., Quon, E., Dana, S., Schreck, S., Raach, S., Haizmann, F., and Schlipf, D.: Full-Scale Field Test of Wake Steering, J. Phys. Conf. Ser., 854, 012 013, https://doi.org/10.1088/1742-6596/854/1/012013, 2017a.

Fleming, P., Annoni, J., Shah, J. J., Wang, L., Ananthan, S., Zhang, Z., Hutchings, K., Wang, P., Chen, W., and Chen, L.: Field test of wake steering at an offshore wind farm, Wind Energy Science, 2, 229–239, https://doi.org/10.5194/wes-2-229-2017, https://www.wind-energ-sci.net/2/229/2017/, 2017b.

Fleming, P., King, J., Dykes, K., Simley, E., Roadman, J., Scholbrock, A., Murphy, P., Lundquist, J. K., Moriarty, P., Fleming, K., van Dam, J., Bay, C., Mudafort, R., Lopez, H., Skopek, J., Scott, M., Ryan, B., Guernsey, C., and Brake, D.: Initial results from a field campaign of wake steering applied at a commercial wind farm – Part 1, Wind Energy Science, 4, 273–285, https://doi.org/10.5194/wes-4-273-2019, https://www.wind-energ-sci.net/4/273/2019/, 2019.

Frandsen, S., Barthelmie, R., Pryor, S., Rathmann, O., Larsen, S., Højstrup, J., and Thøgersen, M.: Analytical modelling of wind speed deficit in large offshore wind farms, Wind Energy, 9, 39–53, https://doi.org/10.1002/we.189, https://onlinelibrary.wiley.com/doi/abs/10.1002/we.189, 2006.

Fuertes, F. C., Markfort, C. D., and Porté-Agel, F.: Wind Turbine Wake Characterization with Nacelle-Mounted Wind Lidars for Analytical Wake Model Validation, Remote Sens., 10, https://doi.org/10.3390/rs10050668, http://www.mdpi.com/2072-4292/10/5/668, 2018.

Gebraad, P. M. O., Teeuwisse, F. W., van Wingerden, J. W., Fleming, P. A., Ruben, S. D., Marden, J. R., and Pao, L. Y.: Wind plant power optimization through yaw control using a parametric model for wake effects—a CFD simulation study, Wind Energy, 19, 95–114, https://doi.org/10.1002/we.1822, https://onlinelibrary.wiley.com/doi/abs/10.1002/we.1822, 2016.

Howland, M. F., Bossuyt, J., Martínez-Tossas, L. A., Meyers, J., and Meneveau, C.: Wake structure in actuator disk models of wind turbines in yaw under uniform inflow conditions, J. Renew. Sustain. Ener., 8, 043 301, https://doi.org/10.1063/1.4955091, https://doi.org/10.1063/1.4955091, 2016.

Jiménez, n., Crespo, A., and Migoya, E.: Application of a LES technique to characterize the wake deflection of a wind turbine in yaw, Wind Energy, 13, 559–572, https://doi.org/10.1002/we.380, https://onlinelibrary.wiley.com/doi/abs/10.1002/we.380, 2009.

Kuo, J. Y., Romero, D. A., Beck, J. C., and Amon, C. H.: Wind farm layout optimization on complex terrains – Integrating a CFD wake model with mixed-integer programming, Appl. Energ., 178, 404 – 414, https://doi.org/https://doi.org/10.1016/j.apenergy.2016.06.085, http://www.sciencedirect.com/science/article/pii/S0306261916308595, 2016.

Lin, M. and Porté-Agel, F.: Large-Eddy Simulation of Yawed Wind-Turbine Wakes: Comparisons with Wind Tunnel Measurements and Analytical Wake Models, Energies, 12, https://doi.org/10.3390/en12234574, https://www.mdpi.com/1996-1073/12/23/4574, 2019.

Lundquist, J. K., Wilczak, J. M., Ashton, R., Bianco, L., Brewer, W. A., Choukulkar, A., Clifton, A., Debnath, M., Delgado, R., Friedrich, K., Gunter, S., Hamidi, A., Iungo, G. V., Kaushik, A., Kosović, B., Langan, P., Lass, A., Lavin, E., Lee, J. C.-Y., McCaffrey, K. L., Newsom, R. K., Noone, D. C., Oncley, S. P., Quelet, P. T., Sandberg, S. P., Schroeder, J. L., Shaw, W. J., Sparling, L., Martin, C. S., Pe, A. S., Strobach, E., Tay, K., Vanderwende, B. J., Weickmann, A., Wolfe, D., and Worsnop, R.: Assessing State-of-the-Art Capabilities for Probing the Atmospheric Boundary Layer: The XPIA Field Campaign, B. Am. Meteorol. Soc., 98, 289–314, https://doi.org/10.1175/BAMS-D-15-00151.1, https://doi.org/10.1175/BAMS-D-15-00151.1, 2017.

Medici, D. and Dahlberg, J. Å.: Potential improvement of wind turbine array efficiency by active wake control (AWC), in: Proc. European Wind Energy Conference and Exhibition, 16-19 June, 2003.

Peña, A., Réthoré, P.-E., and van der Laan, M. P.: On the application of the Jensen wake model using a turbulence-dependent wake decay coefficient: the Sexbierum case, Wind Energy, 19, 763–776, https://doi.org/10.1002/we.1863, https://onlinelibrary.wiley.com/doi/abs/10.1002/we.1863, 2016.

Qian, G.-W. and Ishihara, T.: A New Analytical Wake Model for Yawed Wind Turbines, Energies, 11, https://doi.org/10.3390/en11030665, https://www.mdpi.com/1996-1073/11/3/665, 2018.

Shakoor, R., Hassan, M. Y., Raheem, A., and Wu, Y.-K.: Wake effect modeling: A review of wind farm layout optimization using Jensen's model, Renewable and Sustainable Energy Reviews, 58, 1048 – 1059, https://doi.org/https://doi.org/10.1016/j.rser.2015.12.229, http://www.sciencedirect.com/science/article/pii/S1364032115016123, 2016.

Simley, E., Fleming, P., and King, J.: Design and Analysis of a Wake Steering Controller with Wind Direction Variability, Wind Energy Science Discussions, pp. 1–26, https://doi.org/10.5194/wes-2019-35, 2019.

Simley, E., Fleming, P., and King, J.: Field Validation of Wake Steering Control with Wind Direction Variability, J. Phys. Conf. Ser., 1452, 012 012, https://doi.org/10.1088/1742-6596/1452/1/012012, https://doi.org/10.1088%2F1742-6596%2F1452%2F1%2F012012, 2020.

Stevens, R. J. and Meneveau, C.: Flow Structure and Turbulence in Wind Farms, Annual Review of Fluid Mechanics, 49, 311–339, https://doi.org/10.1146/annurev-fluid-010816-060206, https://doi.org/10.1146/annurev-fluid-010816-060206, 2017.

Thomsen, K. and Sørensen, P.: Fatigue loads for wind turbines operating in wakes, J. Wind Eng. Ind. Aerodyn., 80, 121 – 136, https://doi.org/https://doi.org/10.1016/S0167-6105(98)00194-9, http://www.sciencedirect.com/science/article/pii/S0167610598001949, 1999.

Vasel-Be-Hagh, A. and Archer, C. L.: Wind farms with counter-rotating wind turbines, Sustainable Energy Technologies and Assessments, 24, 19 – 30, https://doi.org/https://doi.org/10.1016/j.seta.2016.10.004, http://www.sciencedirect.com/science/article/pii/S2213138816301072, energy and Water - The Quintessence of Our Future, 2017.

Vermeer, L., Sørensen, J., and Crespo, A.: Wind turbine wake aerodynamics, Prog. Aerosp. Sci., 39, 467 – 510, https://doi.org/https://doi.org/10.1016/S0376-0421(03)00078-2, http://www.sciencedirect.com/science/article/pii/S0376042103000782, 2003.

Vollmer, L., Steinfeld, G., Heinemann, D., and Kühn, M.: Estimating the wake deflection downstream of a wind turbine in different atmospheric stabilities: an LES study, Wind Energy Sci., 1, 129–141, https://doi.org/10.5194/wes-1-129-2016, https://www.wind-energ-sci.net/1/129/2016/, 2016.

Zong, H. and Porté-Agel, F.: A point vortex transportation model for yawed wind turbine wakes, J. Fluid Mech., 890, A8, https://doi.org/10.1017/jfm.2020.123, 2020.